Accepted Manuscript

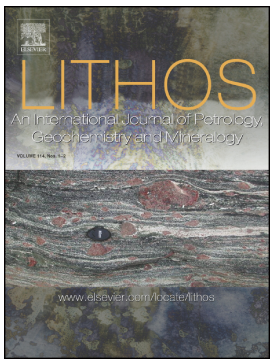

An evaluation of element mobility in the Modderfontein ultramafic complex, Johannesburg: Origin as an Archaean ophiolite fragment or greenstone belt remnant?

George L. Guice, Iain McDonald, Hannah S.R. Hughes, Carl R. Anhaeusser

PII: S0024-4937(19)30083-0
DOI: https://doi.org/10.1016/j.lithos.2019.02.013
Reference: LITHOS 4981

To appear in: *LITHOS*

Received date: 1 November 2018
Accepted date: 16 February 2019

Please cite this article as: G.L. Guice, I. McDonald, H.S.R. Hughes, et al., An evaluation of element mobility in the Modderfontein ultramafic complex, Johannesburg: Origin as an Archaean ophiolite fragment or greenstone belt remnant?, LITHOS, https://doi.org/10.1016/j.lithos.2019.02.013

An evaluation of element mobility in the Modderfontein ultramafic complex, Johannesburg: origin as an Archaean ophiolite fragment or greenstone belt remnant?

George L. Guice[a,*] GuiceG@cardiff.ac.uk, Iain McDonald[a], Hannah S. R. Hughes[b,c], Carl R. Anhaeusser[c]

[a]School of Earth and Ocean Sciences, Cardiff University, Main Building, Park Place, Cardiff, CF10 3AT, UK

[b]Camborne School of Mines, College of Engineering, Mathematics & Physical Sciences, University of Exeter, Penryn Campus, Penryn, Cornwall, TR10 9FE, UK

[c]School of Geosciences, University of the Witwatersrand, Private Bag 3, Wits 2050, Johannesburg South Africa

[*]Corresponding author.

ABSTRACT

The Johannesburg Dome – a tonalite-trondhjemite-granodiorite (TTG)-dominated terrane in the central Kaapvaal Craton – contains a suite of ultramafic-mafic complexes that are concentrated largely along its southern rim. These > 3.3 Ga ultramafic-mafic complexes have recently been re-interpreted as fragments of an Archaean ophiolite (Anhaeusser 2006a), challenging a longstanding hypothesis whereby the complexes represent the intruded remnants of an Archaean greenstone belt. As with similar interpretations of ultramafic-mafic units in other Archaean cratons, the ophiolite hypothesis is used as evidence in favour of Phanerozoic-style plate tectonic processes having operated in the Archaean, with this geodynamic regime the prevailing explanation for the rocks and structures displayed by the Kaapvaal Craton. Through detailed new geological mapping of the scarcely studied Modderfontein Complex, alongside petrography, bulk-rock geochemistry and mineral chemistry, we here assess the validity of both hypotheses. Moreover, having experienced amphibolite-facies metamorphism and substantial hydrothermal alteration, we assess the degree of element mobility experienced by the Modderfontein Complex and discuss the implications for subsequent geodynamic interpretations. The 1 km^2 area mapped comprises separate northern and southern domains, with the former dominated by homogenous serpentinite that contains irregularly-shaped chromitite lenses, and the latter comprising coarsely-layered peridotite, pyroxenite, gabbro and amphibolite. The data indicate that the Modderfontein Complex has experienced significant mobility of Pd, the fluid-mobile lithophile elements (e.g., Ba, Rb and Cs) and potentially some elements generally considered immobile. Mobility of Pd is restricted to chromitite lenses, where Pd was originally hosted by sulphide mineral phases (e.g., pentlandite). This element was immobile in all other Modderfontein lithologies, where it is hosted by nano-scale PGM, demonstrating that PGE mobility is, in-part, controlled by the host phase(s). Moreover, based on a variety of petrographic and geochemical characteristics, including PGE mineralogy and spinel mineral chemistry, it is considered unlikely that the Modderfontein Complex represents an ophiolite

fragment. Instead, the Complex is interpreted as the intrusive remnant of a greenstone belt that was subsequently intruded by TTG magmas.

Keywords: Archaean geodynamics; PGE; Johannesburg Dome; Kaapvaal Craton; chromitite; geochemical fingerprinting; metasomatism

1.0 INTRODUCTION

In recent decades, a Phanerozoic-style plate tectonic framework – involving mid-ocean ridges and subduction in a globally linked system of tectonic plates (Stern 2005, 2008) – has been increasingly applied to rocks of Archaean age (De Wit et al. 1987, 1992, Polat et al. 2009, Gerya et al. 2015), with some authors maintaining that the current geodynamic regime has probably been in operation since 4 Ga (Kusky et al. 2001, Furnes, et al. 2007a, 2007b, Kusky 2010). Other authors state that the distinctive rock associations, geochemical signatures and metamorphic/structural styles of Archaean cratons are inconsistent with Phanerozoic-style plate tectonic processes, with alternative suggestions varying widely (e.g., Van Kranendonk et al. 2004, Bédard 2013, Kamber 2015, Johnson et al. 2017, Smithies et al. 2018, Bédard 2018, Brown and Johnson 2018). For example, Archaean blueschists and paired metamorphic belts, which represent hallmarks of subduction-accretion processes, are absent in Archaean cratons (Stern 2005, 2008, Brown 2008). In response, the proponents of Phanerozoic-style plate tectonic models for the Archaean Earth state that these occurrences were likely destroyed by subsequent overprinting/metamorphic events (e.g., Wyman 2013), and point to the existence of proposed Archaean ophiolites as evidence (e.g., De Wit et al. 1987, Kusky et al. 2001, Furnes, et al. 2007a, Kusky and Li 2008, Dilek and Polat 2008, Furnes et al. 2009, Kusky 2012, Grosch and Slama 2017). Although these Archaean ophiolite occurrences remain highly contested (Bédard et al. 2013, Bédard 2013, Kamber 2015), were they to be unequivocally shown to represent ancient ophiolites, they would provide crucial evidence in favour of Phanerozoic-style plate tectonics having operated during the Archaean (Bédard et al. 2013, Kamber 2015).

The proposed Archaean ophiolites (summarised in Table 1) range in age from 3.8 to 2.5 Ga, cover areas of between 18 and 350 km^2, and comprise a variety of ultramafic to felsic and metasedimentary lithologies that have generally been metamorphosed to amphibolite and/or granulite-facies. For example, the Tartoq Group occurrence, located in the Greenlandic portion of the North Atlantic Craton, comprises pillow lava, gabbro, serpentinite, talc-schist, greenschist and

amphibolite, with all lithologies invaded by tonalite-trondhjemite-granodiorite (TTG) magmas (Table 1; Kisters and Szilas 2012; Szilas et al. 2013; Szilas et al. 2014). Ancient ophiolite interpretations are generally based upon a lithological assemblage that is comparable to Phanerozoic ophiolites (albeit often fragmented and incomplete; Furnes et al. 2009), and occasionally trace-element geochemistry (i.e., the Nb anomaly for suprasubduction zone (SSZ) ophiolites; Yellappa et al. 2012; Table 1). However, residual mantle rocks that exhibit similar geochemical characteristics to those from Phanerozoic ophiolites remain notably absent from proposed Archaean examples, with none of those proposed withstanding detailed investigation (e.g., Szilas et al. 2015, 2018).

The Kaapvaal Craton of South Africa represents one of the oldest (3.6 to 2.7 Ga) and best-preserved portions of lithosphere on Earth (Poujol et al. 2003). The craton, which comprises both TTG gneiss and greenstone belts (Anhaeusser 1973), is generally interpreted to have resulted from the amalgamation of several crustal blocks that nucleated by processes akin to Phanerozoic plate tectonics, although the exact number of blocks and the location of their boundaries remain disputed (Anhaeusser 1973, 1999, De Wit et al. 1992, Poujol et al. 2003, Zeh et al. 2013). While it remains controversial (Hamilton 1998, Van Kranendonk et al. 2014), evidence cited in favour of this interpretation includes the presence of ultramafic-mafic suites, which occur in broadly linear arrays along the northern flank of the Barberton Greenstone Belt, the southern edge of the Johannesburg Dome and the southern edge of the Murchison Greenstone Belt (Viljoen and Viljoen 1970, Anhaeusser 1985, 2006a). These ultramafic-mafic suites comprise a combination of extrusive and intrusive lithologies, with the intrusive complexes sometimes displaying pronounced magmatic differentiation and cyclical layering (Viljoen and Viljoen 1970, Anhaeusser 1977, 1978, 1985, 2001, 2006b). Traditionally, the extrusive rocks were interpreted as representing oceanic plateau assemblages, with the layered complexes representing contemporaneous intrusions that were emplaced at shallow crustal levels and were derived from “komatiitic” magmas (Viljoen and Viljoen 1970). More recently, these ultramafic-mafic suites have been reinterpreted as *ophirags* (ophiolite fragments incorporated into continental crust; Anhaeusser, 2006a) that collectively mark Archaean

suture zone(s), with de Wit et al. (1987) previously interpreting the intrusive ultramafic complexes as mantle rocks.

In this paper, we assess the validity of the previously proposed hypotheses for the origin of the ultramafic-mafic complexes in the Johannesburg Dome and evaluate the effects of element mobility. We present a new geological map, field observations, petrography, bulk-rock geochemistry and mineral chemistry for the Modderfontein Complex, which is a large exposure of ultramafic and mafic rocks located in the eastern Johannesburg Dome (Fig. 1). The only previous (and un-published) mapping of the Modderfontein Complex was conducted by Chaumba (1992), with this mapping area now covered over by urban developments (Fig. 1). Such ongoing urban development continues to drastically reduce exposures of ultramafic and/or mafic rocks in the Johannesburg Dome, with the area studied in this paper (Fig. 1) representing the largest remaining exposure of the Modderfontein Complex at the time of writing.

2.0 REGIONAL GEOLOGY

The Johannesburg Dome – a 700 km^2 basement inlier located in the central domain of the Kaapvaal Craton – is overlain by the Neoarchaean to Neoproterozoic Witwatersrand, Ventersdorp and Transvaal Supergroups, and Phanerozoic Karoo Supergroup (Fig. 1; Poujol et al., 2003). It is dominated by Palaeo- to Mesoarchaean TTG gneiss and contains volumetrically subordinate ultramafic-mafic rocks (Fig. 1; Anhaeusser 1973, 1999, 2006b), with the TTG gneisses derived from a number of magmatic events between 3.34 and 3.11 Ga. The oldest TTG gneiss in the Johannesburg Dome – the 3.34 Ga Lanseria Gneiss – occupies the northern part of the dome (Fig. 1; Robb and Meyer 1995, Barton et al. 1999, Poujol and Anhaeusser 2001). The trondhjemitic and tonalitic magma invaded, fragmented, metamorphosed and migmatised a pre-existing ultramafic-mafic crust that is now manifest as centimetre-scale xenoliths to kilometre-scale remnants enclosed within the Lanseria Gneiss (e.g., Zandspruit; see Anhaeusser, 2015). The 3.20-3.17 Ga hornblende-biotite tonalite (known as the Linden Gneiss; Fig. 1) occupies the southern edge of the Johannesburg Dome

(Barton et al. 1999, Poujol and Anhaeusser 2001, Robb et al. 2006), while the 3.12-3.11 Ga Bryanston, Honeydew and Victory Park granodiorites dominate the remaining southern portions of the Johannesburg Dome (Fig. 1; Poujol and Anhaeusser 2001, Robb et al. 2006). The TTG gneiss and ultramafic-mafic rocks of the Johannesburg Dome are all cross-cut by: numerous ca. 3.0 Ga pegmatites; a suite of 3.12-3.11 Ga, NW-SE to NE-SW-trending lamproite dykes; and a NE-SW-trending shear zone (Fig. 1; Barton et al. 1999, Poujol and Anhaeusser 2001, Prevec et al. 2004, Robb et al. 2006).

A suite of ultramafic-mafic rocks, which is intermittently exposed along the southern rim of the Johannesburg Dome, is exclusively associated with the Linden Gneiss (Fig. 1; Anhaeusser, 2006a,b). Based on field observations and major-element geochemistry, the complexes are interpreted to contain a combination of extrusive (komatiite, basaltic komatiite, high-Mg basalt and tholeiite) and intrusive rocks (peridotite, pyroxenite, gabbro, gabbronorite and norite; Anhaeusser 1977, 1978, 1999, 2006b). Although the ultramafic-mafic rocks have not been directly dated (as is common with Archaean ultramafic rocks; Guice et al. 2018a), field relationships constrain them as older than the local, 3.34 Ga TTG gneiss (Poujol and Anhaeusser 2001, Anhaeusser 2004). The complexes occupy relatively flat, low-lying ground, with serpentinite commonly forming small ridges (Anhaeusser, 2006b). Detailed field descriptions of individual occurrences at Muldersdrift, Roodekrans and Cresta-Robindale (Fig. 1) can be found in Anhaeusser (1977, 1978, 2004, 2006a,b).

3.0 THE MODDERFONTEIN COMPLEX

The Modderfontein Complex (previously referred to as the Edenvale-Modderfontein Complex; Anhaeusser, 2004, 2006b) is a 10 km^2 area of ultramafic and mafic rocks located 10 km NE of the Johannesburg City Centre (Chaumba 1992). This poorly-exposed and scarcely studied complex reportedly contains serpentinite, tremolite-bearing amphibolite and pyroxenite (altered to talc-schist and amphibolite; Chaumba, 1992; Anhaeusser, 2004, 2006b). Steeply-dipping cyclical units of serpentinite and amphibolite – interpreted as representing metamorphosed intrusive rocks

(Anhaeusser 2004, Chaumba 1992) – are reported in the W of the Complex, with serpentinite forming low ridges interspaced with poorly-exposed amphibolite (Anhaeusser 2004). Although the complex has not been directly dated, its age is constrained as older than the cross-cutting 3.34 – 3.20 Ga trondhjemite gneiss on its western side (Poujol and Anhaeusser 2001, Anhaeusser, 2006).

This investigation focuses on a previously un-mapped and un-reported 1 km^2 area in the E of the Modderfontein Complex (Figs. 1 and 2). The exposure is flanked by the R25 road to the N, housing developments to the E and W, and industrial developments to SE and NW (Fig. 2).

3.1 New mapping and field relationships

Mapping of the Modderfontein Complex was conducted in 2016 and utilised Google Earth basemaps and a Garmin eTrex 10 Handheld GPS. Separated by a poorly-exposed and steeply-dipping (70° towards the SW) shear zone that strikes roughly NW-SE, the area can be subdivided into two domains that exhibit distinct lithological assemblages (Fig. 2). The northern domain is dominated by massive serpentinite, while the southern domain comprises layered (on a scale of tens of metres) peridotite, pyroxenite, amphibolite and gabbro (Fig. 2). Ultramafic rocks (serpentinite, peridotite and pyroxenite) generally occur on small hillocks that are better exposed and slightly more vegetated than the surrounding areas (Fig. 3a), while amphibolite and gabbro are poorly-exposed, and occupy the low ground.

3.1.1 Northern Domain

Exposures of massive serpentinite in the NW of the northern domain exhibit distinctly brown weathered surfaces (Fig. 3a), with dark fresh surfaces comprising fine-grained serpentine. In the NW of the domain, serpentinites contain fine-grained magnetite that sporadically forms patches < 2 cm in diameter (Fig. 3b). The SW of the northern domain contains rare, enclaves (on a scale of tens of centimetres) of irregularly-shaped amphibolite that have sharp contacts with the host serpentinite (Fig. 3c). In the SE of the northern domain (Fig. 2), serpentinites contain sporadically distributed and irregularly-shaped chromitite lenses that range from millimetre-scale stringers to centimetre-scale

pods (Fig. 3d-f). Contacts with the host serpentinite are generally sharp (e.g., Fig. 3d), although chromitite is occasionally interspersed with sub-millimetre- to millimetre-scale serpentine patches (e.g., Fig. 3f).

3.1.2 Southern Domain

The southern domain is dominated by peridotite and pyroxenite, with volumetrically subordinate gabbro and amphibolite in the E and W respectively (Fig. 2). The lithological distribution of gabbro, pyroxenite (with subordinate peridotite), peridotite (with subordinate pyroxenite) and amphibolite suggests that this portion of the Modderfontein Complex exhibits NE-SW-trending layering on a scale of tens of metres (Fig. 2). The orientation and scale of such layering is supported by satellite imagery (from 2004) and mapping (Chaumba 1992) of an area of the Modderfontein Complex located 2 km W of the study area (before the area was developed and built upon; see supplementary material). Massive peridotite outcrops are well-exposed and exhibit brown-weathered surfaces, with rare millimetre- to centimetre-scale patches of fine-grained magnetite. The coarse-grained pyroxenites are relatively well-exposed, with millimetre-scale clinopyroxene crystals prominent on the light-brown weathered surfaces. Amphibolites form poorly-exposed, grey-brown outcrops that display a prominent schistosity and light grey fresh surfaces.

4.0 SAMPLES AND ANALYTICAL METHODS

Thirty-two samples were collected in 2016, and of these 21 bulk-rock samples were analysed for major and trace-elements, 7 bulk-rock samples were analysed for platinum-group elements (PGE) and Au, and 14 samples were subject to petrographic analysis. The locations of the analysed samples are detailed in Figure 2b, with grid references provided in the supplementary material.

4.1 Bulk-rock geochemistry

The samples were crushed in a Mn steel jaw-crusher and ground to a fine powder in an agate ball mill, with loss on ignition (LOI) determined gravimetrically. Major and trace-elements were analysed using inductively coupled plasma optical emission spectrometry (ICP-OES) and inductively coupled

plasma mass spectrometry (ICP-MS), with samples prepared using the methods and instrumentation described by McDonald and Viljoen (2006). Accuracy was constrained using international reference materials JB1a, NIM-N, NIM-G and NIM-P, and precision was constrained by analysing duplicates of 5 % of samples. The raw data can be found in Table 2, with duplicate analyses, precision calculations and standard reference materials included in the supplementary material. PGE and Au analyses were conducted using ICP-MS after sample preparation by Ni sulphide fire assay and Te co-precipitation (Huber et al. 2001, McDonald and Viljoen 2006). Accuracy was constrained using international reference materials TDB1, WPR1 and SARM64 (see supplementary material), with PGE and Au analyses included in Table 3.

4.2 Mineral chemistry

Quantitative mineral analyses were conducted at Cardiff University, using a Zeiss Sigma HD Field Emission Gun Analytical Scanning Electron Microscope (A-SEM) equipped with two Oxford Instruments 150 mm^2 EDS detectors. Operating conditions were set at 20kV and analytical drift checks were carried out every 20 minutes using a Co reference standard. The EDS analyser was calibrated using suites of standards from ASTIMEX and Smithsonian, with secondary standard checks performed every hour. Details of the secondary standard checks, including precision calculations, are included in the supplementary material. The raw data were recalculated to element oxide percentages, with Fe^{2+} and Fe^{3+} calculated using the stoichiometric method of Droop (1987). Representative spinel compositions can be found in Table 4, with the full mineral chemical datasets (amphibole, clinopyroxene, feldspar and serpentine and spinel) included in the supplementary material.

5.0 RESULTS

5.1 Petrography

Serpentinites (n= 4; Fig. 4a) comprise (in modal %): > 93 % serpentine and < 7 % tremolite, with accessory magnetite and Cr-spinel. Serpentine grains, which are euhedral to subhedral, elongate and

< 0.1 mm long, collectively represent the serpentinised pseudomorphs of olivine and/or orthopyroxene (Fig. 4a). Fine-grained (< 0.1 mm diameter) magnetite is sporadically distributed between and within serpentine, and occasionally occurs as rounded amalgamations (as seen on the outcrop scale) < 2 mm in diameter. Rounded, 1.5 mm diameter clusters of tremolite are composed of individual, 0.2 to 0.6 mm long, fibrous grains (Fig. 4a).

The serpentinite-hosted lenses of chromitite (n= 1), which occur in the E of the northern domain (Fig. 2), comprise < 0.8 mm diameter, subhedral to euhedral chromite grains (Fig. 4b). On the µm-scale, the chromite grains sometimes appear skeletal, comprising parallel blades of chromite that display sharp boundaries with the surrounding silicate material (see section 5.3 for more details). Such silicate material also forms the boundaries to individual chromite grains (Fig. 4b).

Peridotites (n= 3; Fig. 4c) comprise (in modal %): 55 to 70 % serpentine, 14 to 35 % tremolite and < 31 % relic clinopyroxene, with accessory Cr-spinel and magnetite. Subhedral to anhedral serpentine is fine-grained (< 0.1 mm diameter), with subhedral clinopyroxene < 4 mm in diameter. Relic clinopyroxene is variably replaced by fine-grained (< 0.1 mm diameter) tremolite that may pseudomorph entire clinopyroxene grains, while fine-grained (< 0.15 mm diameter) magnetite is also associated with serpentine as an accessory phase.

Pyroxenites (n= 3; Fig. 4d) comprise (in modal %): 17 to 39 % serpentine, < 2 % amphibole (tremolite and actinolite) and 60 to 81 % (fresh) clinopyroxene, with accessory spinel and magnetite. Large patches of serpentine (< 1 mm diameter), which represent olivine and/or orthopyroxene pseudomorphs, comprise small (< 0.1 mm diameter), subhedral serpentine grains (Fig. 4d) and rare, fine-grained (< 0.3 mm diameter) magnetite (Fig. 4d). Clinopyroxene is subhedral, occasionally altered to tremolite and < 2 mm in diameter (Fig. 4d). Tremolite is randomly distributed within clinopyroxene and forms anhedral grains < 0.2 mm in diameter (Fig. 4d).

One gabbro sample (Fig. 4e) comprises (in modal %): 77.5 % clinopyroxene, 1.5 % amphibole (tremolite and actinolite) and 21 % sericitized plagioclase feldspar. Large (< 3 mm diameter),

subhedral to euhedral clinopyroxene grains exhibit distinctive twinning and limited alteration to tremolite (Fig. 4e). These anhedral to subhedral, < 0.15 mm diameter tremolite grains commonly form rims on clinopyroxene grains (Fig. 4e). Plagioclase is generally highly altered (to sericite), with relic subhedral to anhedral grains appearing to be intercumulus to the clinopyroxene (Fig. 4e).

Amphibolites (n= 2; Fig. 4f) comprise (in modal %): > 90 % amphibole and < 10 % serpentine. Amphiboles are generally anhedral to subhedral and < 0.4 mm in diameter, although larger (< 1 mm diameter) pseudomorphs of clinopyroxene are also preserved. Fine-grained (< 0.15 mm diameter), anhedral serpentine is rare, but occasionally forms large (< 2 mm diameter) pseudomorphs of olivine and/or orthopyroxene (Fig. 4f).

5.2 Bulk-rock geochemistry

5.2.1 Major and minor elements

With the exception of the two samples that contain significant chromite, the serpentinites of the northern domain exhibit relatively restricted ranges in their anhydrous major and minor element compositions, with tight ranges in SiO_2 (42.9 to 45.3 wt. %), TiO_2 (< 0.1 wt. %), Al_2O_3 (0.9 to 3.5 wt. %), Fe_2O_3 (9.1 to 14.7 wt. %), MgO (38.4 to 43.3 wt. %), CaO (< 1.1 wt. %), NiO (0.3 to 0.4 wt. %) and Cr_2O_3 (0.4 to 0.8 wt. %). Relative to these serpentinites, chromitite-bearing serpentinites (7.6 to 9.0 wt. % Cr_2O_3) contain less SiO_2 (33.3 to 33.9 wt. %) and MgO (31.0 to 36.3 wt. %), and more TiO_2 (0.2 to 0.4 wt. %), Al_2O_3 (3.1 to 4.2 wt. %) and Fe_2O_3 (18.0 to 21.2 wt. %). The greater range of lithologies in the southern domain is reflected by their major and minor element compositions (supplementary material), with moderate to broad ranges in SiO_2 (42.3 to 53.0 wt. %), Al_2O_3 (1.8 to 11.8 wt. %), MgO (14.5 to 41.5 wt. %), CaO (1.7 to 11.5 wt. %), Na_2O (0.1 to 0.9 wt. %) and K_2O (< 1.1 wt. %), but tight ranges in TiO_2 (< 0.2 wt. %), Fe_2O_3 (6.9 to 10.6 wt. %), Cr_2O_3 (0.1 to 0.6 wt. %) and NiO (< 0.2 wt. %; Table 2). Collectively, the Modderfontein rocks show significant overlap with the fields for intrusive and extrusive ultramafic-mafic rocks from the Barberton Greenstone Belt, but, importantly, are distinct from those of residual mantle rocks (see supplementary material).

5.2.2 Lithophile trace elements

Except for Hf, the northern domain rocks display poor correlations between Zr and individual elements generally considered immobile (R^2 = < 0.32), and no correlation between Zr and individual elements generally considered mobile (R^2 = < 0.10; Fig. 5). In contrast, the southern domain rocks generally exhibit strong correlations between Zr and Nb, Ti, Ta, Hf and Th (Fig. 5; R^2 = 0.77-1.00), moderate correlations between Zr and Y, Yb and Ho (R^2 = 0.41 – 0.50), and no correlation between Zr and Al_2O_3 (Fig. 5; R^2 = 0.01). These rocks exhibit weak to moderate correlations with the LREE (light rare earth-elements; R^2=0.29-0.51), and no correlation between Zr and other mobile elements (Fig. 5; R^2 = < 0.06).

On chondrite-normalised rare earth-element (REE) plots (Fig. 6a), the northern domain serpentinites exhibit flat heavy-REE (HREE) patterns ($[Gd/Lu]_N$ = 0.7-1.6) and negatively sloping light-REE (LREE) patterns ($[La/Sm]_N$ = 1.4-3.2; $[La/Lu]_N$ = 2.1-5.3), with chondrite-normalised REE abundances ranging from 0.7 to 7.3. On the primitive mantle-normalised trace-element plots (Fig. 6b), these rocks display negatively sloping patterns ($[Th/Yb]_N$ = 4.9-18.2). Within this broad pattern, the incompatible elements show negative slopes ($[Th/Eu]_N$ = 2.5-11.2) and the compatible elements display relatively flat patterns ($[Eu/Yb]_N$ = 0.7-2.7) mostly punctuated by mild negative Nb-Ta-Zr-Hf-Ti anomalies, negative Sr anomalies and positive Ba anomalies. The chromitites display REE and trace-element patterns broadly comparable to the serpentinites (Fig. 6a-b), although these rocks display positive Ti anomalies while the serpentinites show negative Ti anomalies (Fig. 6b).

The southern domain rocks display generally flat REE patterns ($[La/Lu]_N$ = 0.8-3.5), with flat HREE patterns ($[Gd/Lu]_N$ = 0.6-1.3), gently sloping LREE patterns ($[La/Sm]_N$ = 1.3-2.4) and chondrite-normalised REE abundances ranging from 0.9 to 7.1 (Fig. 6c). On primitive mantle-normalised trace-element plots (Fig. 6d), these rocks exhibit generally flat patterns ($[Th/Yb]_N$ = 0.7-4.6) that are punctuated by negative Nb-Ta-Zr-Hf-Ti anomalies, negative Sr anomalies and positive Ba anomalies (Fig. 6d). The one gabbro sample analysed displays a positive Sr anomaly and significant enrichment

in Rb (Fig. 6d). The chondrite-normalised REE and primitive mantle-normalised trace-element compositions of the Modderfontein rocks (both in the northern and southern domains) show significant overlap with the field for intrusive ultramafic-mafic rocks from the Barberton Greenstone Belt and are distinct from the field for ophiolites and abyssal peridotites (Fig. 6a-f).

5.2.3 Platinum-group elements (PGE)

Northern domain serpentinites (n= 3) display mildly fractionated patterns ($[Pd/Ir]_N$ = 1.7-5.0) that exhibit flat Pt-group PGE (PPGE) patterns ($[Pd/Rh]_N$ = 0.5-4.0; Fig. 7a), positive Ru anomalies and positive Au anomalies (Fig. 7a). Relative to these serpentinites, the analysed chromitite-bearing serpentinite (n= 1; Cr_2O_3 = 9.0 wt. %) is enriched in all PGE except Pd by 1-2 orders of magnitude (Fig. 7b). The normalised pattern for this sample is comparatively flat from Ir to Pt ($[Pt/Ir]_N$ = 1.8), with significant depletion in Pd and Au (Fig. 7b). By contrast, the southern domain pyroxenite and peridotite consistently exhibit distinctly fractionated patterns ($[Pd/Ir]_N$ = 8.3-77.7), with positively sloping Ir-group PGE (IPGE) ($[Ru/Os]_N$ = 6.5-11.1), flat to mildly fractionated PPGE ($[Pd/Rh]_N$ = 0.6-4.5) and negative Au anomalies (Fig. 7c-d). Excluding the chromitite-bearing serpentinite sample, the Modderfontein samples show a moderate correlation between Pt and Pd (R^2 = 0.5). However, when the chromitite-bearing serpentinite is included, the Modderfontein samples show no correlation between Pt and Pd (R^2 = 0.1; see supplementary material). The northern domain PGE patterns are comparable to both komatiite and residual mantle fields (Fig. 7a), while the southern domain PGE patterns are IPGE-poor relative to these fields (Fig. 7c-d).

5.3 Platinum-group minerals (PGM)

A total of 20 PGM (summarised in Table 5), which range from 0.4 to 4 µm in diameter and are generally subhedral, were identified in the chromitite sample (for which bulk-rock PGE data are shown in Fig. 7b). Erlichmanite (OsS_2; n= 7), laurite (RuS_2; n= 6) and sperrylite ($PtAs_2$; n= 3) are the dominant PGM species, with individual occurrences of platarsite (PtAsS), platarsite-hollingworthite (PtAsS-RhAsS), hollingworthite-irarsite (RhAsS-IrAsS) and irarsite (IrAsS; Table 5; Fig. 8). The majority

of PGM are associated with chromite grains (n= 13; Fig. 8a-b), with a smaller number associated with silicate-chromite boundaries (n= 3) and silicates (n= 1; Fig. 8c). A further 3 PGM are associated with silicate material located between µm-scale chromite blades (Fig. 8d), with some of the chromite-hosted PGM located within chromite blades (Fig. 8b).

5.4 Spinel mineral chemistry

Additional to secondary magnetite derived from serpentinisation, spinel is present within the chromitite lenses, serpentinite, pyroxenite and peridotite of the Modderfontein Complex. In chromitite lenses, chromite occurs as 0.2 to 0.5 mm diameter, generally subhedral grains that exhibit altered rims. In pyroxenite, peridotite and serpentinite, spinel is generally subhedral to anhedral and ranges from 0.02 to 0.3 mm in diameter, with some grains displaying altered rims < 0.03 mm thick (Fig. 9a-b).

Two-hundred and forty-seven analyses were conducted on spinels from chromitite, serpentine, peridotite and pyroxenite lithologies (Table 4), with spinel compositions subdivided into two populations based on Fe^{3+} numbers (calculated as molar $Fe^{3+}/(Cr+Al+Fe^{3+})$). Group 1 spinels (n= 118) display Fe^{3+} numbers of < 0.35, with group 2 (n= 129) spinels exhibiting Fe^{3+} numbers of > 0.64 (Table 4). Group 1 spinels contain high abundances of MgO, Al_2O_3, TiO_2, MnO and Cr_2O_3, and low abundances of FeO relative to group 2 spinels (Table 4). Group 2 compositions reflect analyses from both spinel cores and altered rims, whereas group 1 spinels were only found from analyses of spinel cores (Fig. 9).

Both spinel populations were assessed according to the key compositional parameters of Barnes and Roeder (2001). Although the composition of the group 1 spinel population is not entirely consistent with any of the established fields of Barnes and Roeder (2001), they plot almost completely within the komatiites field on the Fe^{2+} versus Fe^{3+} diagram (Fig. 10a) and show significant overlap with this field on the Fe^{2+} versus Cr#, Fe^{3+} versus TiO_2 and Cr-Al-Fe^{3+} ternary plots (Fig. 10b-d). The group 1 population also overlaps with the greenschist to amphibolite-facies magnetite rims field on the Fe^{2+}

versus Cr# plot, but is compositionally distinct from this field on all other plots (Fig. 10a-d). This spinel population is compositionally distinct from the layered intrusion field on the Cr-Al-Fe^{3+} plot (Fig. 10d), but shows partial to complete overlap on all other plots (Fig. 10a-c). The group 2 spinel population (Fig. 10e-g) shows partial to complete overlap with the greenschist to amphibolite-facies magnetite rims field on all plots, indicating that they were derived from secondary processes (see Section 6.1.3).

On the Cr_2O_3 versus Al_2O_3 and Cr_2O_3 versus TiO_2 plots (Fig. 11a-b), the composition of group 1 (primary) spinels (from both domains of the Modderfontein Complex) is distinct from those for podiform chromitite, but shows some overlap with the field for stratiform chromitite. On the Al_2O_3 versus TiO_2 plot (Fig.13c), the northern domain group 1 spinels generally fall outside of any established field, with a few analyses plotting within the arc field. In contrast, the southern domain group 1 spinels generally fall within the arc field, but also show some overlap with the suprasubduction zone peridotite and deep mantle chromitite fields (Fig. 11c).

6.0 DISCUSSION

6.1 Effects of metamorphism and element mobility

Like the ultramafic-mafic rocks elsewhere in the Johannesburg Dome (e.g., Anhaeusser, 1977, 1978, 2006a), the Modderfontein Complex has undergone a protracted magmatic and metamorphic history, resulting in amphibolite-facies mineral assemblages and extensive hydrothermal alteration (including serpentinisation). Amphibolite-facies metamorphism and serpentinisation, along with the previously reported invasion of the Modderfontein Complex by TTG magmas (Anhaeusser 2004), are commonly accompanied by metasomatism, including contact metasomatism, diffusion metasomatism and infiltration metasomatism (Barton and Ilchik 1991, Yardley 2013, Guice et al. 2018b). We assess the degree of element mobility experienced by the Modderfontein Complex, to avoid over-interpretation of the geochemical data.

6.1.1 Lithophile element mobility

As indicated by the lack of correlation between Zr and the fluid mobile elements (e.g., Ba, Rb, Cs; Fig. 5), these elements experienced significant mobility in both domains of the Modderfontein Complex – a common effect of serpentinisation (Deschamps et al. 2013). The bivariate plots of Figure 5 also hint at mobility of the LREE and some elements considered immobile in many geological settings, such as Yb, Ho, Y, Al and Ti. While extremely pronounced in the northern domain, this mobility appears negligible in the southern domain, as highlighted by the respective correlations between Zr and these "immobile elements" (and LREE) for the two domains (Fig. 5; section 5.2.2). This apparent element mobility may be the product of melt/rock interaction, as suggested by Deschamps et al. (2013). In this scenario however, LREE mobility by melt/rock interaction must have either exclusively operated in the northern domain or been inefficient in the southern domain (to explain the disparate apparent mobilities in the northern and southern domains), which appears unlikely. Moreover, mapping of the Modderfontein Complex records no evidence of the gradational zonation typically produced by such melt-rock interaction (e.g., Zhou et al. 1996).

Alternatively, the apparent geochemical discrepancy between the two domains of the Modderfontein Complex may be controlled by modal abundances of alteration minerals, which in turn reflect the modal abundance of primary olivine (± orthopyroxene). Comprising > 92 modal % serpentine, the originally high proportions of olivine (± orthopyroxene) in the northern domain rocks amplifies the chemical effects of alteration (including serpentinisation). In contrast, the lower modal abundance of olivine (± orthopyroxene) in the southern domain rocks supress the chemical effects of alteration, leading to a less pronounced apparent mobility of the aforementioned elements (Fig. 12). This interpretation is consistent with the evidence for the mobility of Ba and Cs, which is a common chemical effect of serpentinisation (Deschamps et al. 2013); but may initially appear at odds with the notable depletion in Sr displayed by all-but-one of the Modderfontein samples (Fig. 6), as serpentinisation is commonly associated with Sr-rich fluids that often generate bulk-rock Sr

enrichment (Deschamps et al. 2013). Despite this caveat, we consider the hydrothermal alteration hypothesis to be more likely than the melt/rock interaction hypothesis (Fig. 12).

6.1.2 PGE mineralogy and mobility

The moderately strong positive correlation between Pt and Pd in most samples (section 5.2.3) suggests that these elements were immobile in the majority of the Modderfontein Complex rocks. In the chromitite sample however, Os, Ir, Ru, Rh and Pt concentrations are an order of magnitude higher than the Pd concentration (Fig. 7), suggesting that this sample either: (i) experienced considerable depletion of Pd during secondary processes; or (ii) experienced considerable enrichment of Os, Ir, Ru, Rh and Pt (but not Pd) through either magmatic or hydrothermal processes.

Of the 20 PGM identified in the chromitite sample, 13 are sulphides and 7 are As-bearing phases. Arsenic-bearing PGM species can be the products of either secondary or high temperature processes (e.g., Gauthier et al., 1990; Prichard et al., 1994). The Os and Ru sulphides (erlichmanite and laurite, respectively) on the other hand are nearly always magmatic and, coupled with the absence of any IPGE alloys, are most consistent with relatively high fS_2 conditions and sulphide saturation during formation of the chromitite (Brenan and Andrews 2001, Holwell and McDonald 2007). The close spatial association between sulphide and arsenide-sulpharsenide PGM suggests that many of the latter have either primary or (at least) late-magmatic origin(s) analogous to the high temperature arsenide PGM recorded in settings such as the Great Dyke (Coghill and Wilson 1993), Lavatrafo Complex, Madagascar (McDonald 2008) and Sudbury (Dare et al. 2010). Once formed, these PGM often remain stable during serpentinisation and supergene alteration and may effectively fix the IPGE (+ Rh and Pt) budgets of the rocks even at very high degrees of alteration (Mcdonald et al. 1999, Suárez et al. 2010, Smith et al. 2014).

In sulphide-bearing chromitites, Pd may be accommodated in both PGM and solid solution in pentlandite (Godel et al. 2007, Osbahr et al. 2013, Junge et al. 2014, Holwell and McDonald 2007). Removal of sulphides during alteration, and pentlandite in particular, may potentially liberate

significant amounts of Pd, particularly where semi-metals ligands (to form secondary Pd-PGM) are absent (Holwell et al. 2017). Consequently, we consider it most likely that Pd was preferentially mobilised (and removed) from former (interstitial) sulphides in the chromitite-bearing serpentinite sample during a secondary process(es). As with the lithophile element mobility (Section 6.1.1), it is possible that Pd mobility is associated with the hydrothermal alteration of the Modderfontein Complex, with this suggestion supported by research conducted by Barnes and Liu (2012). These authors suggest that Pd is more soluble than Pt in sulphide mineral phases during hydrothermal alteration, and that it will be more readily mobilised as a result. Moreover, these authors suggest that such mobility can be achieved by relatively low-temperature (~300 °C) hydrothermal fluids (Barnes and Liu 2012), further the supporting the hypothesis that Pd was mobilised by hydrothermal fluids associated with hydrothermal alteration (possibly serpentinisation).

This selective Pd mobility – whereby Pd is immobile in the majority of Modderfontein rocks, but mobile in the chromitite – can likely be attributed to the different mineral phases hosting the PGE in the respective lithologies. In the majority of the Modderfontein rocks, the PGE are probably hosted by nm-scale PGM inclusions in silicate minerals, whereas these elements are demonstrably hosted by PGM sulphide mineral phases (and a primary base metal sulphide assemblage that is now absent) in the chromitite. This hypothesis – whereby the differential mobility of Pd in the Modderfontein rocks is a function of different primary sulphide assemblages (Fig. 12) – is supported the work by Barnes and Liu (2012), who described Pt and Pd as well correlated in S-poor environments, where the PGE are hosted by silicate phases.

6.1.3 Spinel mineral chemistry

Spinel grains are subdivided into two compositionally distinct groups, with group 1 spinels enriched in TiO_2, Al_2O_3, MnO, MgO and Cr_2O_3, and depleted in FeO relative to the group 2 spinels. The group 2 spinel compositions show almost complete overlap with the greenschist- to amphibolite-facies rims field on all plots (Fig. 10e-g; Barnes and Roeder, 2001), demonstrating that they were derived from secondary processes. These altered (group 2) spinel compositions most commonly occur as rims on

group 1 spinels (e.g., Fig. 9a) suggesting that they were derived from alteration of the latter. This alteration led to decreases in the TiO_2, Al_2O_3, MnO, MgO and Cr_2O_3 contents, and increases in the FeO contents of the group 1 spinels. In addition, some group 1 spinels have been completely altered to group 2 compositions (e.g., Fig. 9b; Fig. 12). In contrast, the group 1 spinels are geochemically distinct from those of greenschist- to amphibolite-facies rims, recording compositions that are likely primary and show significant overlap with the komatiite and layered intrusion fields (Fig. 10a-d). It should be noted however, that the group 1 spinels may have experienced some enrichment in the most immobile elements (e.g., Cr and Ti) as a result of the alteration to group 2 compositions, with this process potentially generating some of the observed geochemical scatter within the group 1 compositions.

As spinels are used as a petrogenetic indicator in rocks of various ages and metamorphic grades (Wood 1990, Barnes and Roeder 2001), including in regions that have experienced multiple phases of amphibolite- to granulite-facies metamorphism (Kusky and Jianghai 2010, Szilas et al. 2014, 2015, Guice et al. 2018b), these data demonstrate that a rigorous assessment of spinel texture and composition should be undertaken prior to invoking any such interpretation. Despite the partial- to complete-alteration of spinel grains and significant element mobility identified using the bulk-rock data (see Sections 6.1.1 and 6.1.2), the Modderfontein Complex records spinel compositions that are interpreted as close to primary and that can therefore be utilised to aid petrogenetic interpretations. Consequently, although caution is advised, spinel is an important tool for petrogenetic interpretations in areas that have experienced significant metamorphism, alteration and associated element mobility.

The preceding sections outline the extensive evidence for element mobility experienced by the Modderfontein Complex rocks, further outlining the requirement for rigorous petrographic and geochemical assessments (on a case-by-case basis) prior to applying geochemical-based geodynamic interpretations to Archaean rocks, as demonstrated by several previous authors (Collerson and

Kamber 1999, Condie 2003, 2005, Babechuk and Kamber 2011, Guice et al. 2018b). In the case of the Modderfontein Complex, amphibolite-facies metamorphism led to: recrystallisation of some chromite grains in the serpentinite-hosted chromitite; alteration of spinel compositions to those with higher abundances of Fe_2O_3 and FeO, and lower abundances of TiO_2, Al_2O_3, MnO, MgO and Cr_2O_3; and the amphibolitisation of clinopyroxene to tremolite and cummingtonite (Fig. 12). The subsequent hydrothermal alteration (including serpentinisation) of the Modderfontein Complex had more profound effects on the bulk-rock geochemistry, resulting in (Fig. 12): significant mobility of lithophile elements, including selected elements generally considered immobile; and some removal of Pd and Au from the chromitite-bearing serpentinite. Importantly, our data indicate that the modal % of olivine in the primary Modderfontein Complex rocks controlled the degree of lithophile element mobility, while the mobility of Pd is controlled by its host phase(s).

6.2 Origin and petrogenesis of the Modderfontein Complex

While the origin of the Modderfontein Complex itself has not been previously assessed, the ultramafic-mafic complexes of the Johannesburg Dome have been collectively interpreted as representing either: fragment(s) of an Archaean ophiolite(s) (e.g., Anhaeusser, 2006a); or the intrusive and/or extrusive remnants of Archaean greenstone belts (e.g., Anhaeusser, 1977). The succeeding discussion evaluates the various merits of the two previously proposed hypotheses for the Modderfontein Complex in the context of the data presented in this investigation.

6.2.1 Ophiolite fragment

The distinctive presence of chromitite lenses, which occur in association with the northern domain serpentinites, may be interpreted (based on field observations alone) as podiform chromitites, with this interpretation suggestive of an ophiolitic origin for the Modderfontein Complex. In this scenario, the Complex would represent residual upper mantle, where podiform chromitites commonly form in association with dunite melt channels through peridotite (Arai and Yurimoto 1994, Arai and Miura 2015, 2016). This interpretation is supported by *some* aspects of the PGM mineralogy (Section 5.3),

with 14 of the 20 PGM identified being IPGE-rich species (e.g., erlichmanite, laurite and irarsite; Table 5). This is consistent with podiform chromitites in Phanerozoic ophiolites, which are generally dominated by IPGE-PGM (González-Jiménez et al. 2009b), although PPGE-rich PGM species are prominent in some examples (Tarkian and Prichard 1987, Prichard and Lord 1990, Prichard et al. 1994, Ahmed and Arai 2003). Moreover, laurite-erlichmanite (solid-solution series) is the most common PGM in the Modderfontein Complex, which is also consistent with the Phanerozoic ophiolites generally (Stribrny et al. 2000, Ahmed and Arai 2003, González-Jiménez et al. 2009a). However, this hypothesis is inconsistent with other aspects of the PGM and PGE geochemistry recorded by the Modderfontein Complex. First, although laurite-erlichmanite (solid-solution series) are the most common PGM, ophiolites characteristically contain IPGE alloys that are entirely absent at Modderfontein (Ahmed and Arai 2003, González-Jiménez et al. 2009a). Second, the bulk-rock PGE pattern for the Modderfontein chromitite (Fig. 7) was originally positively fractionated with Rh and Pt enriched over the IPGE (Section 6.1.2), whereas those for ophiolitic chromitite generally exhibit IPGE-rich/PPGE-poor patterns (Barnes et al. 1985). Third, as described in Section 6.1.2, the PGM species are consistent with sulphur-saturation and relatively high fS_2 conditions, with this phenomenon rare in ophiolites.

The residual mantle (ophiolite) hypothesis is also inconsistent with the major- and trace-element geochemical characteristics of the Modderfontein Complex (including those of the chromitite lenses), which are distinct from the established characteristics of residual mantle rocks (Figs. 6-8). First, the composition of the chromite within chromitite lenses is distinct from chromitite within Phanerozoic podiform chromitites (Fig. 11). Relative to Phanerozoic podiform chromitites, the Modderfontein Complex chromitite lenses are depleted in Cr_2O_3 and Al_2O_3, and enriched in TiO_2 (Fig. 11). Second, primary (group 1) spinel from all lithologies (and both domains) is compositionally distinct from the field for ophiolites and oceanic peridotites (Fig. 10). Third, the trace-element abundances displayed by the Modderfontein Complex rocks are at least 2 orders of magnitude greater than those for oceanic mantle residue (Fig. 6), with no evidence for systematic enrichment of

all trace-elements by secondary processes (section 6.1.1). Fourth, the major- and trace-element compositions/trends displayed by the Modderfontein rocks are distinct from those of Phanerozoic ophiolites (Fig. 5; supplementary material). Based on the discussed petrographic and geochemical characteristics, we consider it unlikely that any part of the exposed Modderfontein Complex represents an ophiolite fragment, as proposed by Anhaeusser (2006a).

6.2.2 Intrusive greenstone belt remnant

The coarse grain size of the un-serpentinised lithologies and presence of layering on a scale of tens of metres (Fig. 2) is suggestive of a layered intrusion origin for the Modderfontein Complex, with this interpretation supported by several petrographic and geochemical characteristics. First, 100 % of the PGM identified from the Modderfontein Complex are either PGM sulphides or PGM arsenides, with PGM in layered intrusions generally hosted by either PGM bismuthides, sulphides or arsenides (Stribrny et al. 2000). Second, a significant part of the Pd budget in layered intrusions is hosted by base-metal sulphides such as pentlandite (Godel et al. 2007, Holwell and McDonald 2007, Osbahr et al. 2013, Junge et al. 2014), with a pentlandite-bearing sulphide fraction likely to have been removed from the Modderfontein Complex chromitite by secondary processes (Section 6.1.2). Third, the chondrite-normalised PGE patterns for the Modderfontein Complex are generally mildly to moderately fractionated, which is characteristic of layered intrusions (Barnes et al. 1985). However, this hypothesis is questioned slightly by the composition of spinel, which only shows partial overlap with the stratiform chromitite field on the Cr_2O_3 versus Al_2O_3 plot (Fig. 11a). Despite these small inconsistencies, we consider it most likely that the Modderfontein Complex represents an intrusive complex, whereby the ultramafic-mafic rocks represent metamorphosed and altered cumulates.

The bulk-rock geochemical characteristics described in Section 5.2 indicate that the Modderfontein Complex crystallised from melts derived from moderately high degrees of partial melting (Arndt 2003), with this magmatic affinity suggestive of a greenstone belt association. Rocks from both domains of the Complex show significant overlap with the field for Komatii Formation komatiites on chondrite-normalised REE and primitive mantle-normalised trace-element plots (Fig. 6). Further, the

Modderfontein rocks often display compositions and trends comparable to those shown by Komatii Formation komatiites on major-element bivariate plots (supplementary material). Finally, the composition of spinel shows consistent overlap with the previously established field for komatiites (Fig. 10; Barnes and Roeder 2001). These characteristics are consistent with an interpretation whereby the Modderfontein Complex represents the intrusive remnant of an Archaean greenstone belt, supporting the original suggestion of Anhaeusser (1977, 1978), who interpreted the Johannesburg Dome ultramafic-mafic complexes as various intrusive and/or extrusive remnants of an Archaean greenstone belt.

7.0 SUMMARY AND CONCLUSIONS

The mapped portion of the Modderfontein Complex comprises lithologically distinctive northern and southern domains that are separated by a discrete, NW-SE-trending shear zone. The northern domain, which is dominated by massive serpentinites, contains irregularly-shaped, millimetre- to centimetre-scale lenses of chromitite. Although field relationships suggest that these chromitite lenses may represent Archaean podiform chromitite, this hypothesis is inconsistent with the PGM, bulk-rock geochemistry and spinel mineral chemistry. The southern domain comprises volumetrically dominant peridotite and pyroxenite, and volumetrically subordinate gabbro and amphibolite, with these lithologies coarsely layered on a scale of tens of metres. The Modderfontein Complex preserves amphibolite-facies mineral assemblages and has experienced significant hydrothermal alteration, leading to significant mobility of Pd, the fluid-mobile elements (e.g., Ba, Rb and Cs) and potentially some elements considered immobile (e.g., the LREE). Mobility of Pd is restricted to chromitite lenses, where Pd was likely hosted by sulphide mineral phases (e.g., pentlandite). This element was immobile in all other Modderfontein lithologies, where it is hosted by nano-scale PGM, demonstrating that PGE mobility is, in-part, controlled by the host phase(s). Based on several petrographic and geochemical characteristics, we consider it unlikely that the Modderfontein Complex represents an ophiolite fragment, as previously proposed for the ultramafic-mafic

complexes of the Johannesburg Dome (Anhaeusser, 2006a). Instead, our detailed geochemical and petrographic investigation suggests that the Modderfontein Complex most likely represents part of a layered intrusion that crystallised from a magma derived from high degrees of partial melting. Consequently, it is likely that that the Complex represents the intrusive remnant of an Archaean greenstone belt, as initially proposed for the ultramafic-mafic complexes of the Johannesburg Dome (Anhaeusser, 1977).

ACKNOWLEDGEMENTS AND FUNDING

GLG would like to thank the Society of Economic Geologists (Graduate Fellowship Award) and Geological Society (Timothy Jefferson Fund) for extremely generous grants that funded the lead author's fieldwork in Johannesburg. GLG would also like to thank K. Dalton, S. Prawn and M. Donze for field assistance during the summer of 2016; T. Oldroyd for timely production of high quality thin sections; and D. Muir for A-SEM training, advice and assistance. We thank editor M. Scambelluri, and C. Harris and one anonymous reviewer for constructive reviews that helped to improve the quality of this manuscript.

REFERENCES

Ahmed, A.H. and Arai, S. (2003) 'Platinum-Group Minerals in Podiform Chromitites of the Oman Ophiolite'. *Canadian Mineralogist* 41 (3), 597–616

Anhaeusser, C.R. (2015) 'Metasomatized and Hybrid Rocks Associated with a Palaeoarchaean Layered Ultramafic Intrusion on the Johannesburg Dome, South Africa'. *Journal of African Earth Sciences* 102, 203–217

Anhaeusser, C.R. (2006a) 'A Reevaluation of Archean Intracratonic Terrane Boundaries on the Kaapvaal Craton, South Africa: Collisional Suture Zones?' *Geological Society of America, Special Paper* 405, 193–210

Anhaeusser, C.R. (2006b) 'Mafic and Ultramafic Intrusions of the Kaapvaal Craton'. *The Geology of South Africa* 95–134

Anhaeusser, C.R. (2004) 'Palaeoarchaean to Mesoproterozoic (c. 3500 - 1000 Ma) Ultramafic and Mafic Intrusions of the Kaapvaal Craton and Neighbouring Metamorphic Belts: A Review'. *Econ. Geol. Res. Unit, Univ. Witwatersrand, Johannesburg* 384

Anhaeusser, C.R. (2001) 'The Anatomy of an Extrusive-Intrusive Archaean Mafic-Ultramafic Sequence: The Nelshoogte Schist Belt and Stolzburg Layered Ultramafic Complex, Barberton Greenstone Belt, South Africa'. *South African Journal of Geology* 104 (2), 167–204

Anhaeusser, C.R. (1999) 'Archaean Crustal Evolution of the Central Kaapval Craton, South Africa: Evidence from the Johannesburg Dome'. *South African Journal of Geology* 102 (4), 303–322

Anhaeusser, C.R. (1985) 'Archaean Layered Ultramafic Complexes in the Barberton Mountain Land, South Africa'. *Special Paper for the Geological Association of Canada* 28, 281–320

Anhaeusser, C.R. (1978) 'The Geology and Geochemistry of the Muldersdrif Ultramafic Complex, Krugersdorp District'. *Trans. Geol. Soc. S. Afr.* 81, 193–203

Anhaeusser, C.R. (1977) 'Geological and Geochemical Investigations of the Roodekrans Ultramafic Complex and Surrounding Archaean Volcanic Rocks, Krugersdorp District'. *Transactions of the Geological Society of South Africa* 80, 17–28

Anhaeusser, C.R. (1973) 'The Geology and Geochemistry of the Archaean Granites and Gneisses of the Johannesburg-Petoria Dome'. *Special Publication of the Geological Society of South Africa* 3, 361–385

Arai, S. and Miura, M. (2016) 'Formation and Modification of Chromitites in the Mantle'. *Lithos* 264, 277–295

Arai, S. and Miura, M. (2015) 'Podiform Chromitites Do Form beneath Mid-Ocean Ridges'. *Lithos* 232, 143–149

Arai, S., Uesugi, J., and Ahmed, A.H. (2004) 'Upper Crustal Podiform Chromitite from the Northern Oman Ophiolite as the Stratigraphically Shallowest Chromitite in Ophiolite and Its Implication for Cr Concentration'. *Contributions to Mineralogy and Petrology* 147, 145–154

Arai, S. and Yurimoto, H. (1994) 'Podiform Chromitites of the Tari-Misaka Ultramarie Complex, Southwestern Japan, as Mantle-Melt Interaction Products'. *Economic Geology* 89, 1279–1288

Arndt, N. (2003) 'Komatiites, Kimberlites, and Boninites'. *Journal of Geophysical Research: Solid Earth* [online] 108 (B6), 1–11. available from <http://doi.wiley.com/10.1029/2002JB002157>

Babechuk, M.G. and Kamber, B.S. (2011) 'An Estimate of 1.9 Ga Mantle Depletion Using the High-Field-Strength Elements and Nd–Pb Isotopes of Ocean Floor Basalts, Flin Flon Belt, Canada'. *Precambrian Research* 189 (1–2), 114–139

Barnes, S.J. and Liu, W. (2012) 'Pt and Pd Mobility in Hydrothermal Fluids: Evidence from Komatiites and from Thermodynamic Modelling'. *Ore Geology Reviews* 44, 49–58

Barnes, S.J., Naldrett, A.J., and Gorton, M.P. (1985) 'The Origin of the Fractionation of Platinum-Group Elements in Terrestrial Magmas'. *Chemical Geology* 53 (3–4), 303–323

Barnes, S.J. and Roeder, P.L. (2001) 'The Range of Spinel Compositions in Terrestrial Mafic and Ultramafic Rocks'. *Journal of Petrology* 42 (12), 2279–2302

Barton, J.M., Barton, E.S., and Kröner, A. (1999) 'Age and Isotopic Evidence for the Origin of the Archaean Granitoid Intrusives of the Johannesburg Dome, South Africa'. *Journal of African Earth Sciences* 28 (3), 693–702

Barton, M.D. and Ilchik, R.P. (1991) 'Metasomatism'. in *Contact Metamorphism, Vol. 26. Mineralogical Society of America*. ed. by Kerrick, D.M. 321–350

Bédard, J.H. (2018) 'Stagnant Lids and Mantle Overturns: Implications for Archaean Tectonics, Magma Genesis, Crustal Growth, Mantle Evolution, and the Start of Plate Tectonics'. *Geoscience Frontiers* 9 (1), 19–49

Bédard, J.H. (2013) 'How Many Arcs Can Dance on the Head of a Plume? A "comment" on: A Critical Assessment of Neoarchean "Plume Only" Geodynamics: Evidence from the Superior Province, by Derek Wyman, Precambrian Research, 2012'. *Precambrian Research* 229, 189–197

Bédard, J.H., Harris, L.B., and Thurston, P.C. (2013) 'The Hunting of the SnArc'. *Precambrian Research* 229, 20–48

Blichert-Toft, J. and Arndt, N.T. (1999) 'Hf Isotope Compositions of Komatiites'. *Earth and Planetary Science Letters* 171 (3), 439–451

Brenan, J.M. and Andrews, D. (2001) 'Higher-Temperature Stability of Laurite and Ru-Os-Lr Alloy and Their Role in PGE Fractionation in Mafic Magmas'. *Canadian Mineralogist* 39 (2), 341–360

Brévart, O., Dupré, B., and Allègre, C.J. (1986) 'Lead-Lead Age of Komatiitic Lavas and Limitations on the Structure and Evolution of the Precambrian Mantle'. *Earth and Planetary Science Letters* 77 (3–4), 293–302

Brown, M. (2008) 'Characteristic Thermal Regimes of Plate Tectonics and Their Metamorphic Imprint throughout Earth History: When Did Earth First Adopt a Plate Tectonic Mode of Behavior?' *The Geological Society of America, Special Paper* 440, 97–113

Brown, M. and Johnson, T.E. (2018) 'Secular Change in Metamorphism and the Onset of Global Plate Tectonics'. *American Mineralogist* 103 (2), 181–196

Chaumba, J.B. (1992) *The Geology and Geochemistry of Part of the Edenvale Granite-Greenstone Terrane, Johannesburg-Pretoria Granite Dome (BSc (Hons) Thesis)*. Univ. Witwatersrand, Johannesburg

Chavagnac, V. (2004) 'A Geochemical and Nd Isotopic Study of Barberton Komatiites (South Africa):

Implication for the Archean Mantle'. *Lithos* 75 (3–4), 253–281

Cloete, M. (1999) 'Aspects of Volcanism and Metamorphism of the Onverwacht Group Lavas in the South-Western Portion of the Barberton Greenstone Belt'. *Memoirs of the Geological Survey of South Africa* 84, 232

Coghill, B.M. and Wilson, A.H. (1993) 'Platinum-Group Minerals in the Selukwe Subchamber, Great Dyke, Zimbabwe - Implications for Pge Collection Mechanisms and Post-Formational Redistribution'. *Mineralogical Magazine* 57 (389), 613–633

Collerson, K.D. and Kamber, B.S. (1999) *Evolution of the Continents and the Atmosphere Inferred from Th-U-Nb Systematics of the Depleted Mantle*. 283 (March), 1519–1523

Condie, K.C. (2005) 'TTGs and Adakites: Are They Both Slab Melts?' *Lithos* 80 (1–4 SPEC. ISS.), 33–44

Condie, K.C. (2003) 'Incompatible Element Ratios in Oceanic Basalts and Komatiites: Tracking Deep Mantle Sources and Continental Growth Rates with Time'. *Geochemistry, Geophysics, Geosystems* 4 (1), 1–28

Dare, S.A.S., Barnes, S.J., and Prichard, H.M. (2010) 'The Distribution of Platinum Group Elements (PGE) and Other Chalcophile Elements among Sulfides from the Creighton Ni-Cu-PGE Sulfide Deposit, Sudbury, Canada, and the Origin of Palladium in Pentlandite'. *Mineralium Deposita* 45 (8), 765–793

Deschamps, F., Godard, M., Guillot, S., Hattori, K., Deschamps, F., Godard, M., Guillot, S., and Hattori, K. (2013) 'Geochemistry of Subduction Zone Serpentinites: A Review'. *Lithos* 178 (March), 96–127

Dilek, Y. and Polat, A. (2008) 'Suprasubduction Zone Ophiolites and Archean Tectonics'. *Geology* 36 (5), 431–432

Droop, G.T.R. (1987) 'A General Equation for Estimating Fe3+ Concentrations in Ferromagnesian Silicates and Oxides from Microprobe Analyses, Using Stoichiometric Criteria'. *Mineralogical Magazine* 51 (361), 431–435

Friend, C.R.L. and Nutman, A.P. (2010) 'Eoarchean Ophiolites? New Evidence for the Debate on the

Isua Supracrustal Belt, Southern West Greenland'. *American Journal of Science* 310, 826–861

Furnes, H., Robins, B., and De Wit, M.J. (2012) 'Geochemistry and Petrology of Lavas in the Upper Onverwacht Suite, Barberton Mountain Land, South Africa'. *South African Journal of Geology* 115 (2), 171–210

Furnes, H., Rosing, M., Dilek, Y., and de Wit, M. (2009) 'Isua Supracrustal Belt (Greenland)-A Vestige of a 3.8 Ga Suprasubduction Zone Ophiolite, and the Implications for Archean Geology'. *Lithos* 113 (1–2), 115–132

Furnes, H., de Wit, M., Staudigel, H., Rosing, M., and Muehlenbachs, K. (2007a) 'A Vestige of Earth's Oldest Ophiolite'. *Science* 315 (5819), 1704–1707

Furnes, H., de Wit, M., Staudigel, H., Rosing, M., and Muehlenbachs, K. (2007b) 'Response to Comments on "A Vestige of Earth's Oldest Ophiolite"'. *Science* 318 (5851), 746e–746e

Gauthier, M., Corrivaux, L., Trottier, L.J., and Bortholomew, I.D. (1990) 'Chromitites Platiniferes Des Complexes Ophiolitiques de l'Estrie - Beauce, Appalaches Du Sud Du Quebec'. *Mineralium Deposita* 25 (169–178)

Gerya, T. V., Stern, R.J., Baes, M., Sobolev, S. V., Whattam, S.A., and Gerya, T. V. (2015) 'Plate Tectonics on the Earth Triggered by Plume-Induced Subduction Initiation'. *Nature* [online] 527 (7577), 221–225. available from <http://dx.doi.org/10.1038/nature15752>

Godard, M., Jousselin, D., and Bodinier, J. (2000) 'Relationships between Geochemistry and Structure beneath a Palaeo-Spreading Centre: A Study of the Mantle Section in the Oman Ophiolite'. *Earth and Planetary Science Letters* 180, 133–148

Godard, M., Lagabrielle, Y., Alard, O., and Harvey, J. (2008) 'Geochemistry of the Highly Depleted Peridotites Drilled at ODP Sites 1272 and 1274 (Fifteen-Twenty Fracture Zone, Mid-Atlantic Ridge): Implications for Mantle Dynamics beneath a Slow Spreading Ridge'. *Earth and Planetary Science Letters* 267, 410–425

Godel, B., Barnes, S.J., and Maier, W.D. (2007) 'Platinum-Group Elements in Sulphide Minerals, Platinum-Group Minerals, and Whole-Rocks of the Merensky Reef (Bushveld Complex, South

Africa): Implications for the Formation of the Reef'. *Journal of Petrology* 48 (8), 1569–1604

González-Jiménez, J.M., Gervilla, F., Proenza, J. a., Augé, T., and Kerestedjian, T. (2009a) 'Distribution of Platinum-Group Minerals in Ophiolitic Chromitites'. *Applied Earth Science : IMM Transactions Section B* 118 (3), 101–110

González-Jiménez, J.M., Gervilla, F., Proenza, J.A., Augé, T., and Kerestedjian, T. (2009b) 'Distribution of Platinum-Group Minerals in Ophiolitic Chromitites'. *Applied Earth Science: IMM Transactions Section B* 118 (3), 101–110

Google Earth (2016) *Greenstone Hill. 26°07'14.34"S, 28°09'05.75"E. Accessed 1st June 2016*.

Greber, N.D., Puchtel, I.S., Nägler, T.F., and Mezger, K. (2015) 'Komatiites Constrain Molybdenum Isotope Composition of the Earth's Mantle'. *Earth and Planetary Science Letters* 421, 129–138

Grosch, E.G. and Slama, J. (2017) 'Evidence for 3.3-Billion-Year-Old Oceanic Crust in the Barberton Greenstone Belt, South Africa'. *Geology* 45 (7), 1–4

Guice, G.L., McDonald, I., Hughes, H., Schlatter, D., Goodenough, K., MacDonald, J., and Faithfull, J. (2018a) 'Assessing the Validity of Negative High Field Strength-Element Anomalies as a Proxy for Archaean Subduction: Evidence from the Ben Strome Complex, NW Scotland'. *Geosciences* 8 (9), 338

Guice, G.L., McDonald, I., Hughes, H.S.R., MacDonald, J.M., Blenkinsop, T.G., Goodenough, K.M., Faithfull, J.W., and Gooday, R.J. (2018b) 'Re-Evaluating Ambiguous Age Relationships in Archean Cratons: Implications for the Origin of Ultramafic-Mafic Complexes in the Lewisian Gneiss Complex'. *Precambrian Research* 311, 136–156

Hamilton, W.B. (1998) 'Archean Magmatism and Deformation Were Not Products of Plate Tectonics'. *Precambrian Research* 91 (1–2), 143–179

Hanghòj, K., Kelemen, P.B., Hassler, D., Godard, M., Hanghøj, K., Kelemen, P.B., Hassler, D., and Godard, M. (2010) 'Composition and Genesis of Depleted Mantle Peridotites from the Wadi Tayin Massif, Oman Ophiolite; Major and Trace Element Geochemistry, and Os Isotope and PGE Systematics'. *Journal of Petrology* 51 (1–2), 201–227

Hoffmann, J.E., Münker, C., Polat, A., König, S., Mezger, K., and Rosing, M.T. (2010) 'Highly Depleted Hadean Mantle Reservoirs in the Sources of Early Archean Arc-like Rocks, Isua Supracrustal Belt, Southern West Greenland'. *Geochimica et Cosmochimica Acta* 74 (24), 7236–7260

Hofmann, A. and Harris, C. (2008) 'Silica Alteration Zones in the Barberton Greenstone Belt: A Window into Subseafloor Processes 3.5-3.3 Ga Ago'. *Chemical Geology* 257 (3–4), 224–242

Holwell, D.A. and McDonald, I. (2007) 'Distribution of Platinum-Group Elements in the Platreef at Overysel, Northern Bushveld Complex: A Combined PGM and LA-ICP-MS Study'. *Contributions to Mineralogy and Petrology* 154 (2), 171–190

Holwell, D.A., Mitchell, C.L., Howe, G.A., Evans, D.M., Ward, L.A., and Friedman, R. (2017) 'The Munali Ni Sulfide Deposit , Southern Zambia : A Multi-Stage , Megabreccia'. *Ore Geology Reviews*

Huber, H., Koeberl, C., McDonald, I., and Reimold, W.U. (2001) 'Geochemistry and Petrology of Witwatersrand and Dwyka Diamictites from South Africa: Search for an Extraterrestrial Component'. *Geochimica et Cosmochimica Acta* 65 (12), 2007–2016

Johnson, T.E., Brown, M., Gardiner, N.J., Kirkland, C.L., and Smithies, R.H. (2017) 'Earth's First Stable Continents Did Not Form by Subduction'. *Nature* 543, 239

Junge, M., Wirth, R., Oberthür, T., Melcher, F., and Schreiber, A. (2014) 'Mineralogical Siting of Platinum-Group Elements in Pentlandite from the Bushveld Complex, South Africa'. *Mineralium Deposita* 50 (1), 41–54

Kamber, B.S. (2015) 'The Evolving Nature of Terrestrial Crust from the Hadean, through the Archaean, into the Proterozoic'. *Precambrian Research* 258, 48–82

Kamenetsky, V.S., Crawford, A.J., and Meffre, S. (2001) 'Factors Controlling Chemistry of Magmatic Spinel : An Empirical Study of Associated Olivine, Cr-Spinel and Melt Inclusions from Primitive Rocks'. *Journal of Petrology* 42 (4), 655–671

Kisters, A.F.M. and Szilas, K. (2012) 'Geology of an Archaean Accretionary Complex – The Structural Record of Burial and Return Flow in the Tartoq Group of South West Greenland'. *Precambrian*

Research 220–221 (November), 107–122

Van Kranendonk, M.J., Collins, W.J., Hickman, A., and Pawley, M.J. (2004) 'Critical Tests of Vertical vs. Horizontal Tectonic Models for the Archaean East Pilbara Granite-Greenstone Terrane, Pilbara Craton, Western Australia'. *Precambrian Research* 131 (3–4), 173–211

Van Kranendonk, M.J., Kröner, A., Hoffmann, J.E., Nagel, T., and Anhaeusser, C.R. (2014) 'Just Another Drip : Re-Analysis of a Proposed Mesoarchean Suture from the Barberton Mountain Land, South Africa'. *Precambrian Research* 254, 19–35

Kusky, T.M. (2012) 'The Neoarchean Ophiolite in the North China Craton : Early Precambrian Plate Tectonics and Scientific Debate'. *Journal of Earth Science* 23 (3), 277–284

Kusky, T.M. and Jianghai, L. (2010) 'Origin and Emplacement of Archean Ophiolites of the Central Orogenic Belt , North China Craton'. *Journal of Earth Science* 21 (5), 744–781

Kusky, T.M., Li, J., and Tucker, R.D. (2001) 'The Archean Dongwanzi Oceanic Crust and Mantle'. *Science* 292 (May), 1142–1146

Kusky, T.M. and Li, J.H. (2008) 'Note on the Paper by Guochun Zhao , Simon A . Wilde , Sanzhong Li , Min Sun , Matthew L . Grant and Xuping Li , 2007 , " U – Pb Zircon Age Constraints on the Dongwanzi Ultramafic – Mafic Body , North China, Confirm It Is Not an Archean Ophiolite "'. *Earth and Planetary Science Letters* 273, 227–230

Kusky, T.M., Zhi, X., Li, J., Xia, Q., Raharimahefa, T., and Huang, X. (2007) 'Chondritic Osmium Isotopic Composition of Archean Ophiolitic Mantle, North China Craton'. *Gondwana Research* 12, 67–76

Lahaye, Y., Arndt, N., Byerly, G., Chauvel, C., Fourcade, S., and Gruau, G. (1995) 'The Influence of Alteration on the Trace-Element and Nd Isotopic Compositions of Komatiites'. *Chemical Geology* 126, 43–64

Lodders, K. (2003) 'Solar System Abundances and Condensation Temperatures of the Elements'. *The Astrophysical Journal* 591 (2), 1220–1247

Luguet, A., Lorand, J.-P., and Seyler, M. (2003) 'Sulfide Petrology and Highly Siderophile Element Geochemistry of Abyssal Peridotites: A Coupled Study of Samples from the Kane Fracture Zone

(45° W 23°20N , MARK Area , Atlantic Ocean)'. *Geochemica et Cosmochimica Acta* 67 (8), 1553–1570

Maier, W.D. (2003) 'The Concentration of the Platinum-Group Elements in South African Komatiites: Implications for Mantle Sources, Melting Regime and PGE Fractionation during Crystallization'. *Journal of Petrology* 44 (10), 1787–1804

McDonald, I. (2008) 'Platinum-Group Element and Sulphide Mineralogy in Ultramafic Complexes at Western Andriamena, Madagascar'. *Applied Earth Science* 117 (1), 1–10

Mcdonald, I., Ohnenstetter, D., and Vaughan, D.J. (1999) 'Palladium Oxides in Ultramafic Complexes near Lavatrafo,Western Andriamena, Madagascar'. *Mineralogical Magazine* 63 (3), 345–352

McDonald, I. and Viljoen, K.S. (2006) 'Platinum-Group Element Geochemistry of Mantle Eclogites: A Reconnaissance Study of Xenoliths from the Orapa Kimberlite, Botswana'. *Applied Earth Science* 115 (3), 81–93

McDonough, W.F. and Sun, S. s. (1995) 'The Composition of the Earth'. *Chemical Geology* 120 (3–4), 223–253

Ordóñez-calderón, J.C., Polat, A., Fryer, B.J., Appel, P.W.U., Gool, J.A.M. Van, Dilek, Y., and Gagnon, J.E. (2009) 'Geochemistry and Geodynamic Origin of the Mesoarchean Ujarassuit and Ivisaartoq Greenstone Belts , SW Greenland'. *Lithos* 113 (1–2), 133–157

Osbahr, I., Klemd, R., Oberthür, T., Brätz, H., and Schouwstra, R. (2013) *Platinum-Group Element Distribution in Base-Metal Sulfides of the Merensky Reef from the Eastern and Western Bushveld Complex , South Africa*. 211–232

Parman, S.W., Shimizu, N., Grove, T.L., and Dann, J.C. (2003) 'Constraints on the Pre-Metamorphic Trace Element Composition of Barberton Komatiites from Ion Probe Analyses of Preserved Clinopyroxene'. *Contributions to Mineralogy and Petrology* 144 (4), 383–396

Paulick, H., Bach, W., Godard, M., Hoog, J.C.M. De, Suhr, G., and Harvey, J. (2006) 'Geochemistry of Abyssal Peridotites (Mid-Atlantic Ridge , 15°20'N, ODP Leg 209): Implications for Fluid/Rock Interaction in Slow Spreading Environments'. *Chemical Geology* 234, 179–210

Polat, A., Appel, P.W.U., Fryer, B., Windley, B., Frei, R., Samson, I.M., and Huang, H. (2009) 'Trace Element Systematics of the Neoarchean Fiskenaesset Anorthosite Complex and Associated Meta-Volcanic Rocks, SW Greenland: Evidence for a Magmatic Arc Origin'. *Precambrian Research* 175 (1–4), 87–115

Polat, A., Frei, R., Appel, P.W.U., Dilek, Y., Fryer, B., Ordóñez-Calderón, J.C., and Yang, Z. (2008) 'The Origin and Compositions of Mesoarchean Oceanic Crust: Evidence from the 3075 Ma Ivisaartoq Greenstone Belt, SW Greenland'. *Lithos* 100 (1–4), 293–321

Poujol, M. and Anhaeusser, C.R. (2001) 'The Johannesburg Dome, South Africa: New Single Zircon U-Pb Isotopic Evidence for Early Archaean Granite-Greenstone Development within the Central Kaapvaal Craton'. *Precambrian Research* 108 (1–2), 139–157

Poujol, M., Robb, L.J., Anhaeusser, C.R., and Gericke, B. (2003) 'A Review of the Geochronological Constraints on the Evolution of the Kaapvaal Craton, South Africa'. *Precambrian Research* 127 (1–3), 181–213

Prevec, S.A., Poujol, M., Craton, K., Africa, S., Prevec, S.A., Anhaeusser, C.R., and Poujol, M. (2004) 'Evidence for Archaean Lamprophyre from the Kaapvaal Craton, South Africa'. *South African Journal of Science* 100 (August 2015), 549–555

Prichard, H.M., Ixer, R.A., Lord, R.A., Maynard, J., and Williams, N. (1994) 'Assemblages of Platinum-Group Minerals and Sulfides in Silicate Lithologies and Chromite-Rich Rocks within the Shetland Ophiolite'. *Canadian Mineralogist* 32 (2), 271–294

Prichard, H.M. and Lord, R.A. (1990) 'Platinum and Palladium in the Troodos Ophiolite Complex, Cyprus'. *Canadian Mineralogist* 28, 607–617

Puchtel, I.S., Blichert-Toft, J., Touboul, M., Walker, R.J., Byerly, G.R., Nisbet, E.G., and Anhaeusser, C.R. (2013) 'Insights into Early Earth from Barberton Komatiites: Evidence from Lithophile Isotope and Trace Element Systematics'. *Geochimica et Cosmochimica Acta* 108, 63–90

Puchtel, I.S., Walker, R.J., Touboul, M., Nisbet, E.G., and Byerly, G.R. (2014) 'Insights into Early Earth from the Pt-Re-Os Isotope and Highly Siderophile Element Abundance Systematics of Barberton

Komatiites'. *Geochimica et Cosmochimica Acta* 125, 394–413

Robb, L.J., Brandl, G., and Poujol, M. (2006) 'Archaean Granitoid Intrusions'. in *Geology of South Africa*. 57–94

Robb, L.J. and Meyer, F.M. (1995) 'The Witwatersrand Basin, South Africa: Geological Framework and Mineralization Processes'. *Ore Geology Reviews* 10, 67–94

Robin-Popieul, C.C.M., Arndt, N.T., Chauvel, C., Byerly, G.R., Sobolev, A. V., and Wilson, A. (2012) 'A New Model for Barberton Komatiites: Deep Critical Melting with High Melt Retention'. *Journal of Petrology* 53 (11), 2191–2229

Robins, B., Sandstå, N.R., Furnes, H., and de Wit, M. (2010) 'Flow Banding in Basaltic Pillow Lavas from the Early Archean Hooggenoeg Formation, Barberton Greenstone Belt, South Africa'. *Bulletin of Volcanology* 72 (5), 579–592

Rollinson, H. (2008) 'The Geochemistry of Mantle Chromitites from the Northern Part of the Oman Ophiolite : Inferred Parental Melt Compositions'. *Contributions to Mineralogy and Petrology* 156, 273–288

Smith, J.W., Holwell, D.A., and McDonald, I. (2014) 'Precious and Base Metal Geochemistry and Mineralogy of the Grasvally Norite–Pyroxenite–Anorthosite (GNPA) Member, Northern Bushveld Complex, South Africa: Implications for a Multistage Emplacement'. *Mineralium Deposita* 49 (6), 667–692

Smithies, R.H., Ivanic, T.J., Lowrey, J.R., Morris, P.A., Barnes, S.J., Wyche, S., and Lu, Y. (2018) 'Two Distinct Origins for Archean Greenstone Belts'. *Earth and Planetary Science Letters* 487, 106–116

Stern, R.J. (2008) 'Modern-Style Plate Tectonics Began in Neoproterozoic Time: An Alternative Interpretation of Earth's Tectonic History'. *Special Publication of the Geological Society of America* 440, 265–280

Stern, R.J. (2005) 'Evidence from Ophiolites, Blueschists, and Ultrahigh-Pressure Metamorphic Terranes That the Modern Episode of Subduction Tectonics Began in Neoproterozoic'. *Geology*

33 (7), 557–560

Stribrny, B., Wellmer, F.-W., Burgath, K.-P., Oberthür, T., Tarkian, M., and Pfeiffer, T. (2000) 'Unconventional PGE Occurrences and PGE Mineralization in the Great Dyke: Metallogenic and Economic Aspects'. *Mineralium Deposita* 35 (2–3), 260–280

Suárez, S., Prichard, H.M., Velasco, F., Fisher, P.C., and Mcdonald, I. (2010) *Alteration of Platinum-Group Minerals and Dispersion of Platinum-Group Elements during Progressive Weathering of the Aguablanca Ni – Cu Deposit , SW Spain*. 331–350

Szilas, K., van Hinsberg, V., Mcdonald, I., Næraa, T., Rollinson, H., Adetunji, J., Bird, D., Hinsberg, V. Van, Mcdonald, I., Næraa, T., Rollinson, H., Adetunji, J., and Bird, D. (2018) 'Highly Refractory Archaean Peridotite Cumulates: Petrology and Geochemistry of the Seqi Ultramafic Complex, SW Greenland'. *Geoscience Frontiers* 9 (3), 689–714

Szilas, K., Van Hinsberg, V.J., Creaser, R.A., Kisters, A.F.M.M., Hinsberg, V. Van, and Kisters, A.F.M.M. (2014) 'The Geochemical Composition of Serpentinites in the Mesoarchaean Tartoq Group, SW Greenland: Harzburgitic Cumulates or Melt-Modified Mantle?' *Lithos* 198–199 (1), 103–116

Szilas, K., Hinsberg, V.J. Van, Kisters, A.F.M., Hoffmann, J.E., Windley, B.F., Kokfelt, T.F., Scherstén, A., Frei, R., Rosing, M.T., and Münker, C. (2013) 'Remnants of Arc-Related Mesoarchaean Oceanic Crust in the Tartoq Group of SW Greenland'. *Gondwana Research* 23 (2), 436–451

Szilas, K., Kelemen, P.B., and Bernstein, S. (2015) 'Peridotite Enclaves Hosted by Mesoarchaean TTG-Suite Orthogneisses in the Fiskefjord Region of Southern West Greenland'. *GeoResJ* 7, 22–34

Tarkian, M. and Prichard, H.M. (1987) 'Irarsite-Hollingworthite Solid-Solution Series and Other Associated Ru-, Os-, Ir-, and Rh-Bearing PGM's from the Shetland Ophiolite Complex'. *Mineralium Deposita* 22 (3), 178–184

Thompson Stiegler, M., Cooper, M., Byerly, G.R., and Lowe, D.R. (2012) 'Geochemistry and Petrology of Komatiites of the Pioneer Ultramafic Complex of the 3.3Ga Weltevreden Formation, Barberton Greenstone Belt, South Africa'. *Precambrian Research* 212–213, 1–12

Viljoen, M.J. and Viljoen, R.P. (1969) 'Evidence for the Existence of a Mobile Extrusive Peridotitic

Magma from the Kamoti Formation of the Onverwacht Group'. *Special Publication of the Geological Society of South Africa* 2, 87–112

Viljoen, R.P. and Viljoen, M.J. (1970) 'The Geology and Geochemistry of the Layered Ultramafic Bodies of the Kaapmuiden Area, Barberton Mountain Land'. *The Geological Society of South Africa, Special Publication* 1

De Wit, M.J., Hart, R.A., and Hart, R.J. (1987) 'The Jamestown Ophiolite Complex, Barberton Mountain Belt: A Section through 3.5 Ga Oceanic Crust'. *Journal of African Earth Sciences* 6 (5), 681–730

De Wit, M.J., De Ronde, C.E.J., Tredoux, M., Roering, C., Hart, R.J., Armstrong, R.A., Green, R.W.E., Peberdy, E., and Hart, R.A. (1992) 'Formation of an Archaean Continent'. *Nature* 357 (6379), 553–562

Wood, B.J. (1990) 'An Experimental Test of the Spinel Peridotite Oxygen Barometer'. *Journal of Geophysical Research* 95 (B10), 15845–15851

Wyman, D.A. (2013) 'A Reply to "How Many Arcs Can Dance on the Head of a Plume?" By Jean Bedard, Precambrian Research, 2012'. *Precambrian Research* [online] 229, 198–202. available from <http://dx.doi.org/10.1016/j.precamres.2012.08.010>

Yardley, B.W.D. (2013) 'The Chemical Composition of Metasomatic Fluids in the Crust'. in *Metasomatism and the Chemical Transformation of Rock: The Role of Fluids in Terrestrial and Extraterrestrial Processes*. Springer, London, 17–51

Yellappa, T., Santosh, M., Chetty, T.R.K., Kwon, S., Park, C., Nagesh, P., Mohanty, D.P., and Venkatasivappa, V. (2012) 'A Neoarchean Dismembered Ophiolite Complex from Southern India: Geochemical and Geochronological Constraints on Its Suprasubduction Origin'. *Gondwana Research* 21 (1), 246–265

Zeh, A., Jaguin, J., Poujol, M., Boulvais, P., Block, S., and Paquette, J.L. (2013) 'Juvenile Crust Formation in the Northeastern Kaapvaal Craton at 2.97Ga-Implications for Archean Terrane Accretion, and the Source of the Pietersburg Gold'. *Precambrian Research* 233, 20–43

Zhao, G., Wilde, S.A., Li, S., Sun, M., Grant, M.L., and Li, X. (2008) 'Response to Note on " U – Pb Zircon Age Constraints on the Dongwanzi Ultramafic – Mafic Body , North China, Confirm It Is Not an Archean Ophiolite " by Kusky and Li'. *Earth and Planetary Science Letters* 273, 231–234

Zhao, G., Wilde, S.A., Li, S., Sun, M., Grant, M.L., and Li, X. (2007) 'U – Pb Zircon Age Constraints on the Dongwanzi Ultramafic – Mafic Body, North China , Confirm It Is Not an Archean Ophiolite'. *Earth and Planetary Science Letters* 255, 85–93

Zhou, M.F., Robinson, P.T., Malpas, J., and Li, Z. (1996) 'Podiform Chromitites in the Luobusa Ophiolite (SouthernTibet) :Implications for Melt-Rock Interaction and Chromite Segregation in the Upper Mantle'. *Journal of Petrology* 37 (1), 3–21

FIGURES AND CAPTIONS

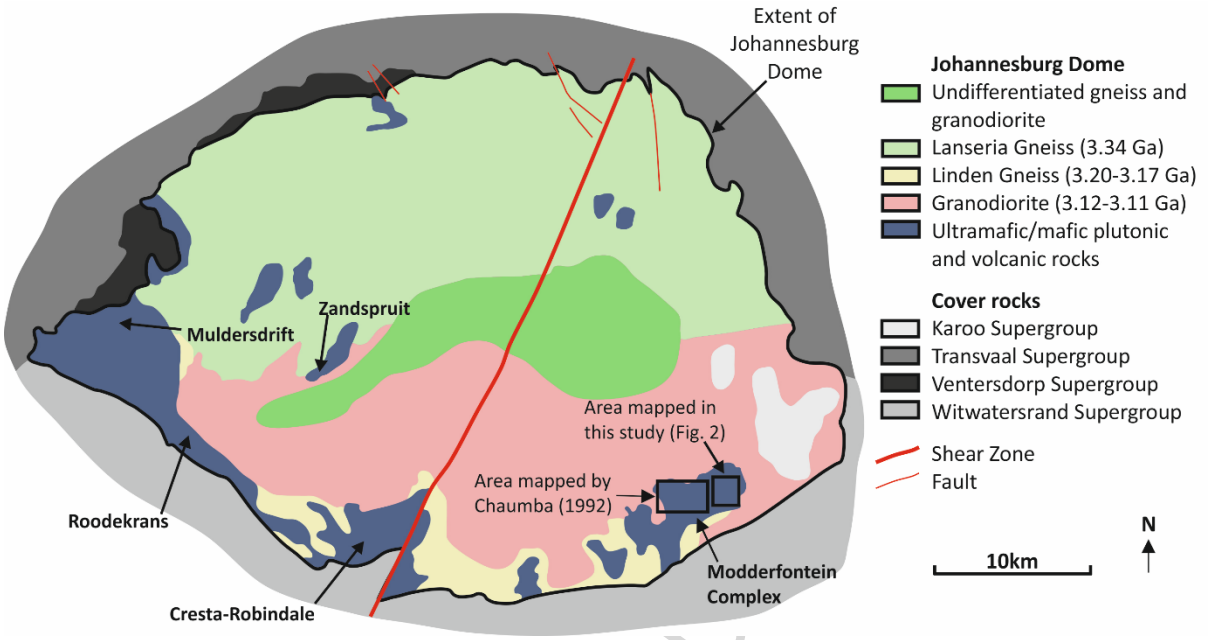

Fig. 1: Simplified geological map of the Johannesburg Dome, detailing the spatial distribution of ultramafic-mafic rocks (redrawn after: Poujol and Anhaeusser 2001, Anhaeusser 2006b, Robb et al. 2006, Anhaeusser 2015).

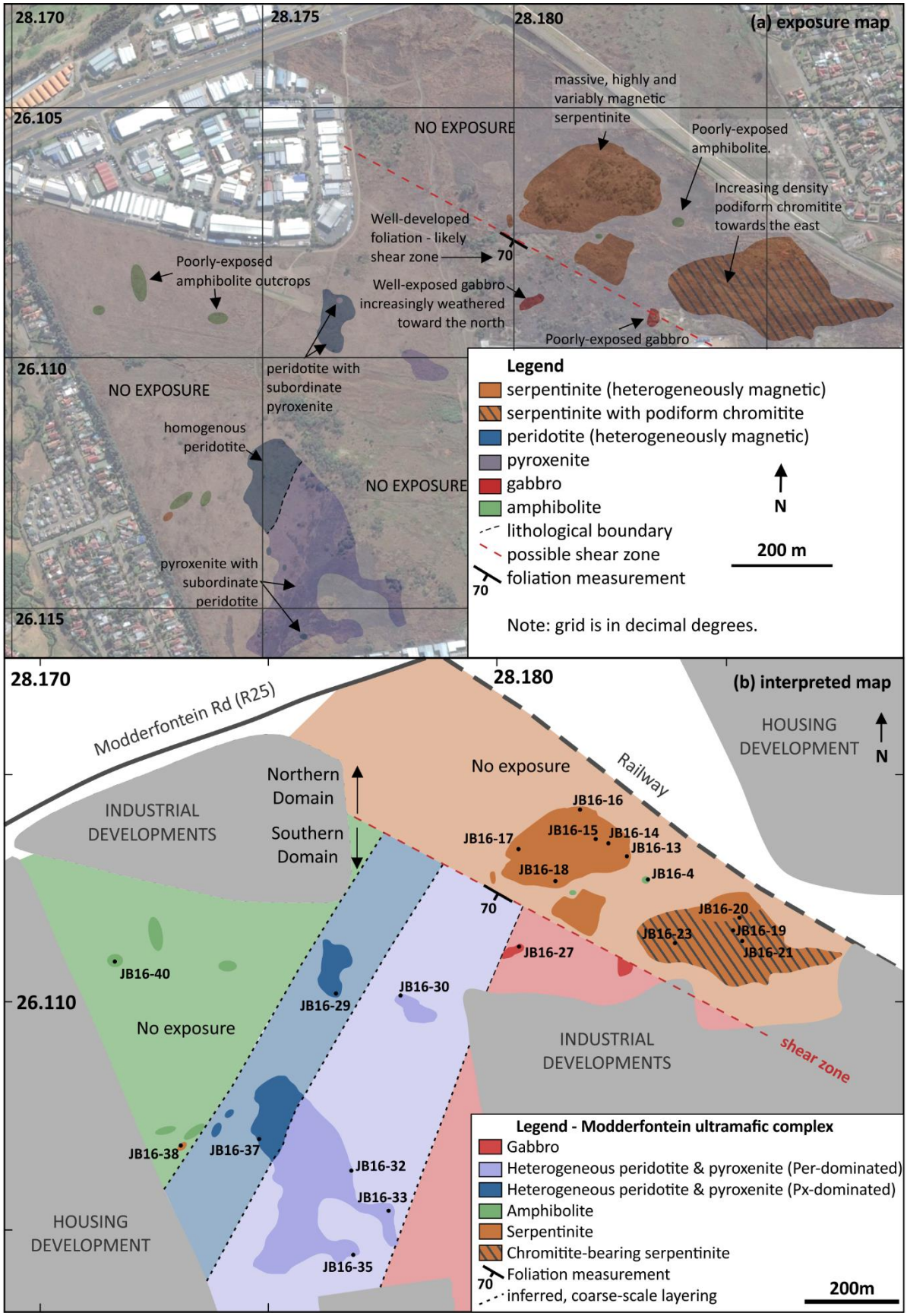

Fig. 2: (a) Exposure map of studied portion of the Modderfontein Complex. Satellite imagery from Google Earth (2016); (b) Interpreted geological map of the Modderfontein Complex, detailing sample locations (black dots and associated text) and distribution of exposures (represented by the darker colours). Grid references are in decimal degrees (coordinate system: WGS1984) and geographical features are in grey.

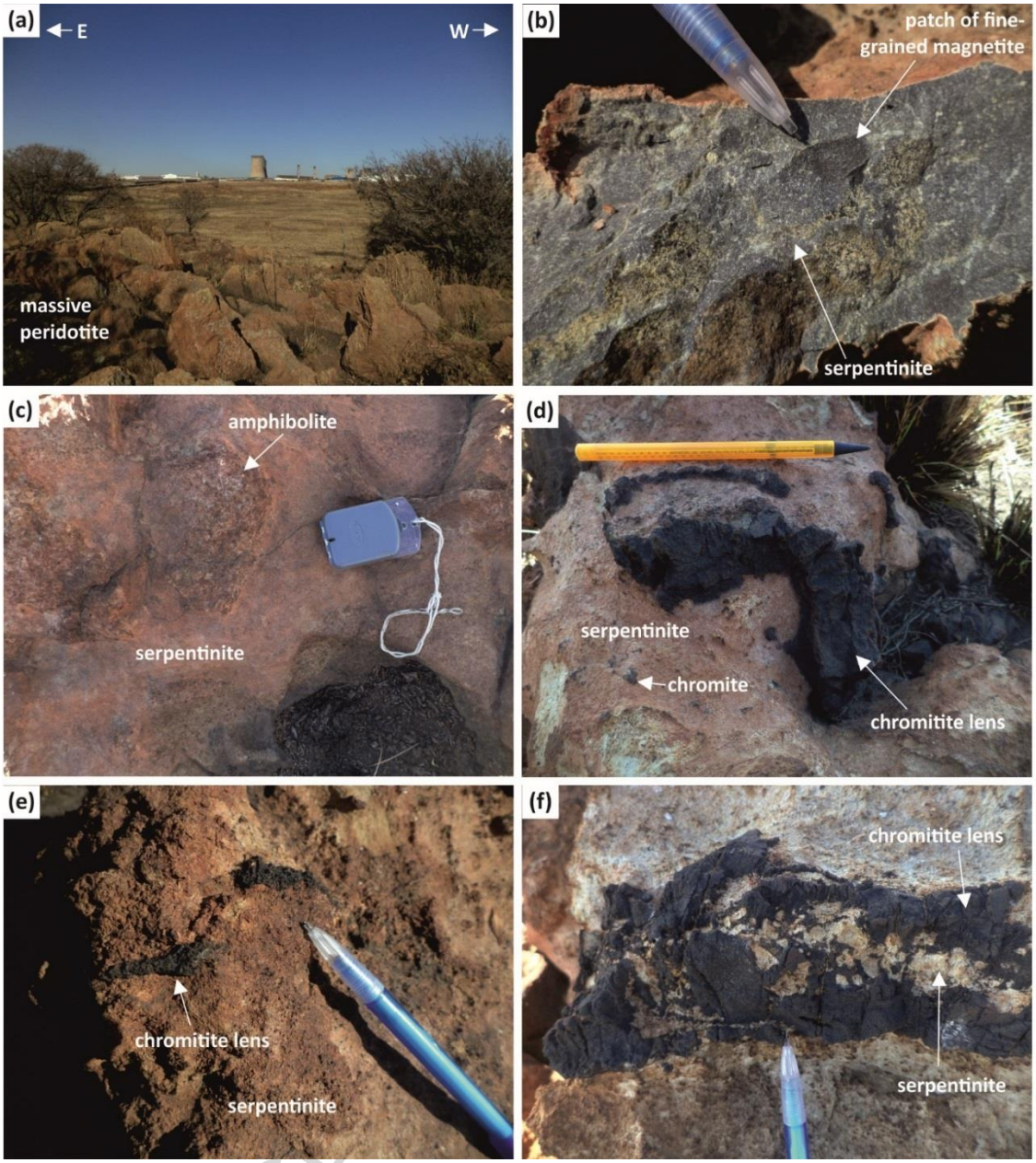

Fig. 3: Field photographs from the Modderfontein Complex. (a) massive peridotite forming a small hillock in the NW of the northern domain. (b) millimetre-scale patches of fine-grained magnetite in serpentinite from the NW of the northern domain. (c) decimetre-scale enclave of amphibolite within serpentinite in the SW of the northern domain. (d) decimetre-scale chromitite lens in the SE of the northern domain. Note sharp contacts with surrounding serpentinite. (e) millimetre-scale lenses of chromitite in the SE of the northern domain. (f) irregularly-shaped, centimetre-scale chromitite lens in the SE of the northern domain, exhibiting interspersed chromitite and serpentinite. Pencil length = 15 cm; compass length = 10 cm.

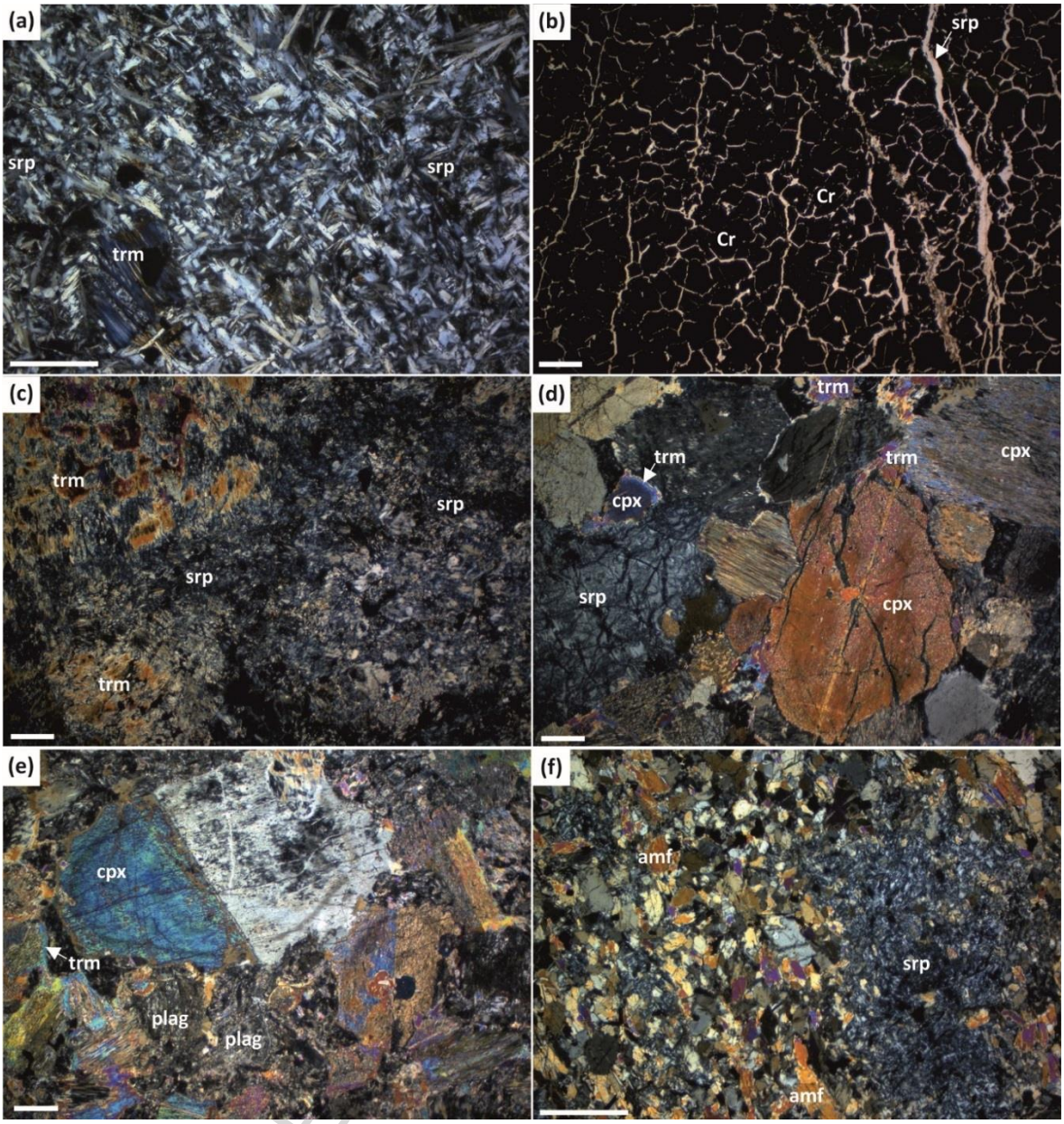

Fig. 4: Photomicrographs detailing the petrographic characteristics of the Modderfontein Complex rocks. All photomicrographs were taken using crossed-polarised light, with the exception of (b), which was taken using plane-polarised light. (a) fine-grained serpentinite containing 500 µm diameter patch of tremolite, from the northwest of the northern domain; (b) podiform chromite from the E of the northern domain; (c) peridotite from the southern domain, containing serpentine and tremolite; (d) pyroxenite from the southern domain, comprising coarse-grained clinopyroxene, minor tremolite, and serpentine pseudomorphs of olivine and/or orthopyroxene; (e) gabbro from the southern domain, comprising clinopyroxene, minor tremolite and interstitial plagioclase; (f)

amphibolite from the W of the southern domain, containing fine-grained amphibole (tremolite and actinolite) and a rare serpentine pseudomorph. amf = amphibole; Cr = chromite; cpx = clinopyroxene; plag = plagioclase; srp = serpentine; trm = tremolite; white scale bar = 500 µm.

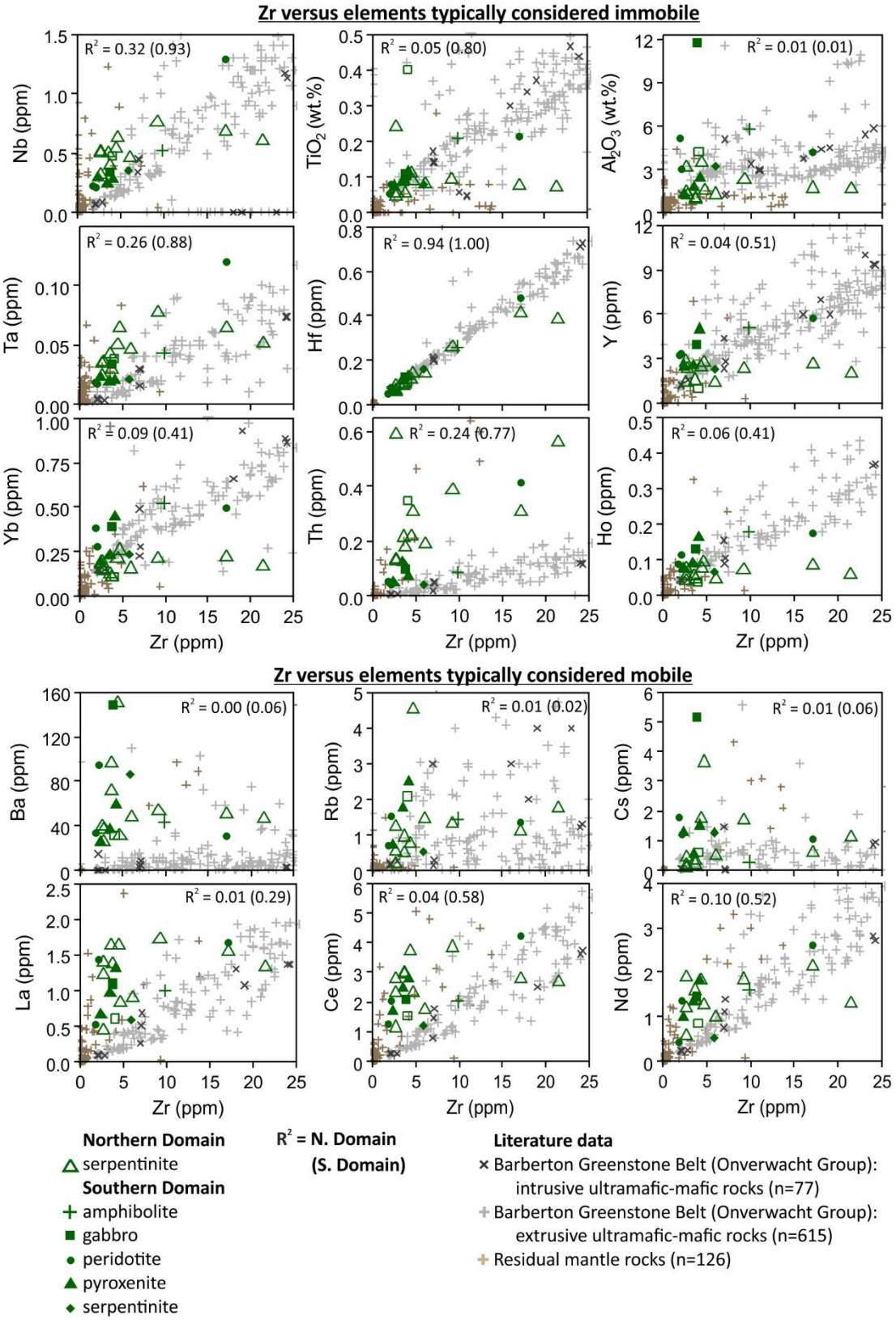

Fig. 5: Bivariate plots detailing the trace-element geochemistry of the Modderfontein rocks. The studied Modderfontein rocks are compared to: extrusive mafic-ultramafic rocks from the Onverwacht Group of the Barberton Greenstone Belt (data from: Brévart et al. 1986, De Wit et al. 1987, Lahaye et al. 1995, Cloete 1999, Blichert-Toft and Arndt 1999, Anhaeusser 2001, Maier 2003, Parman et al. 2003, Chavagnac 2004, Hofmann and Harris 2008, Robins et al. 2010, Thompson Stiegler et al. 2012, Robin-Popieul et al. 2012, Puchtel et al. 2013, Greber et al. 2015); intrusive mafic-ultramafic rocks from the Barberton Greenstone Belt (data from: Viljoen and Viljoen 1969, De Wit et al. 1987, Anhaeusser 2001, Chavagnac 2004, Furnes et al. 2012, Robin-Popieul et al. 2012); and residual mantle rocks from Phanerozoic ophiolites and abyssal peridotites (data from: Godard et al. 2000, Paulick et al. 2006, Godard et al. 2008).

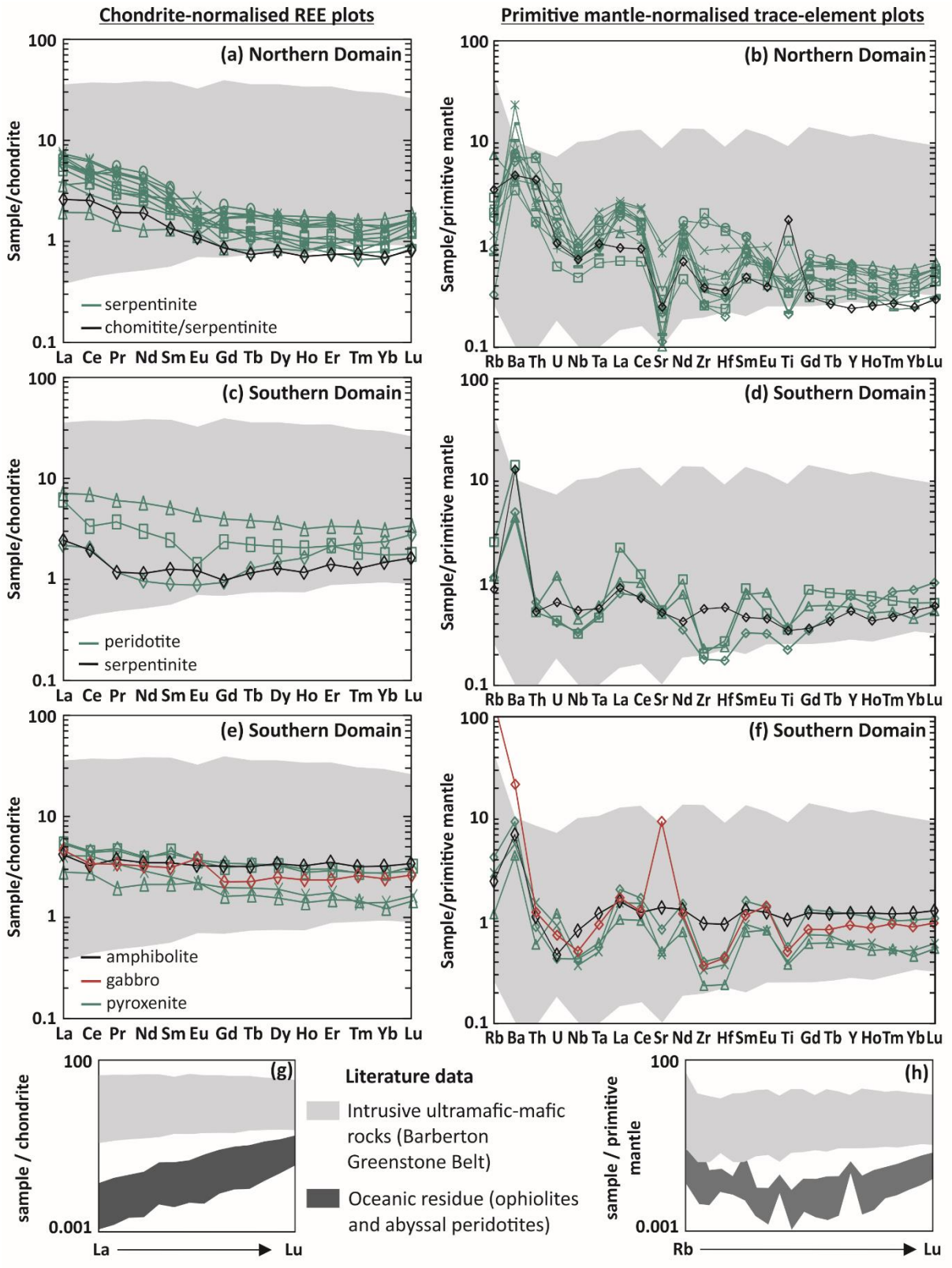

Fig. 6: Chondrite-normalised rare earth-element and primitive mantle-normalised (McDonough and Sun 1995) trace-element plots for the Modderfontein Complex. The data for the intrusive-ultramafic-mafic rocks are from the Barberton Greenstone Belt (Robin-Popieul et al. 2012, Furnes et

al. 2012), while the oceanic residue field is for abyssal peridotites (Paulick et al. 2006, Godard et al. 2008) and ultramafic rocks within the Oman Ophiolite (Godard et al. 2000).

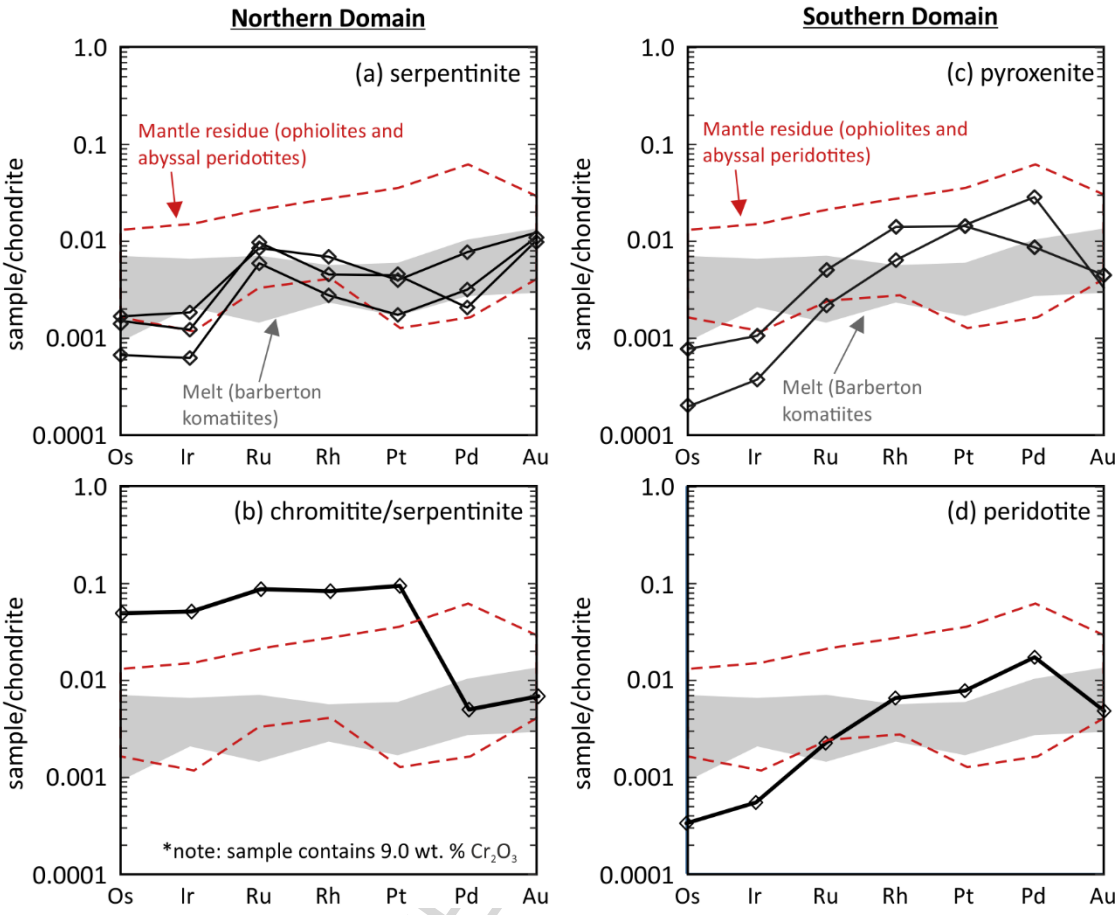

Fig. 7: Chondrite-normalised (Lodders 2003) platinum group-element patterns for the Modderfontein Complex. Melt data are for Barberton Greenstone Belt (Komatii Formation) komatiites (Maier 2003, Puchtel et al. 2014). Mantle residue data are for abyssal peridotites (Luguet et al. 2003) and ultramafic mantle rocks from the Oman ophiolite (Hanghòj et al. 2010).

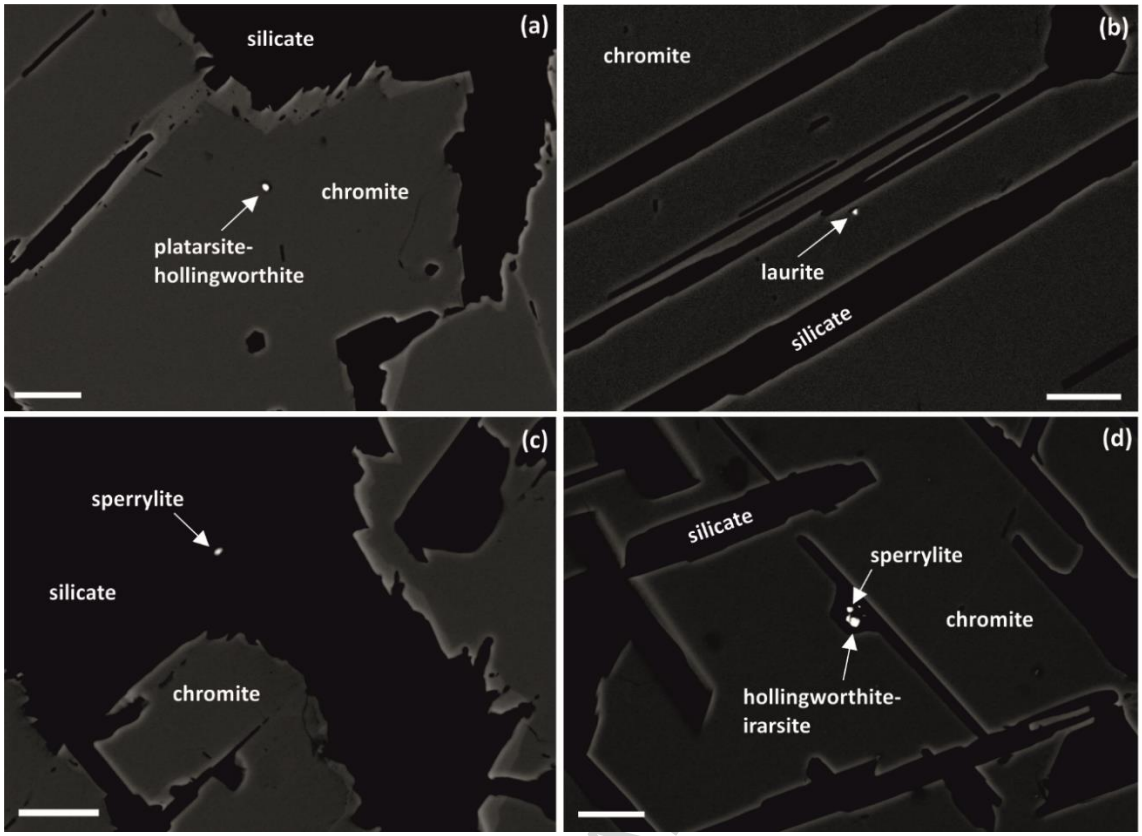

Fig. 8: Back-scattered electron images detailing the morphology of representative platinum-group minerals from the Modderfontein chromitite. (a) chromite-hosted platarsite-hollingworthite grain; (b) laurite grain hosted by chromite blade; (c) silicate-hosted (Al-rich serpentine) sperrylite; (d) separate sperrylite and hollingworthite-irarsite grains hosted by the silicate material (Al-rich serpentine) between a skeletal chromite. White scale bar = 10 µm.

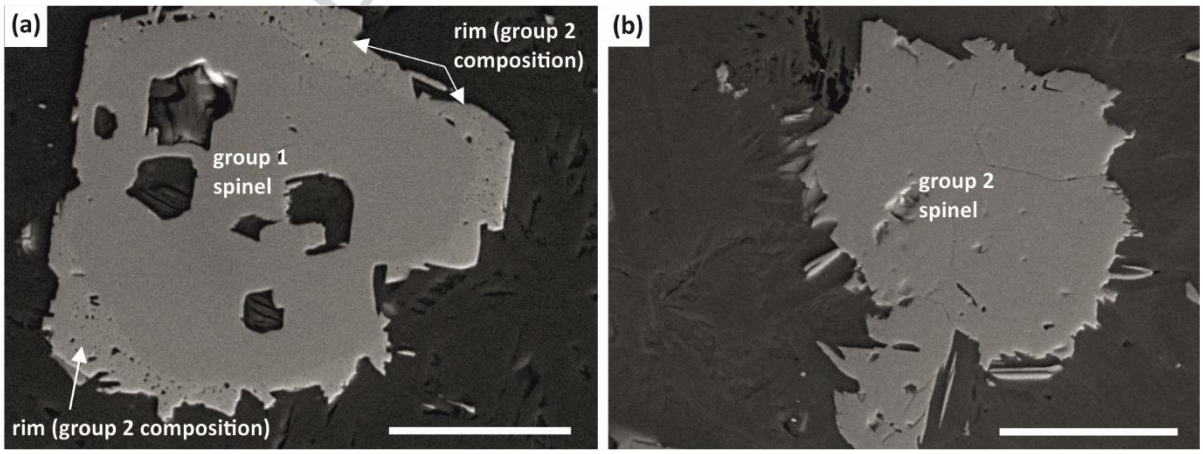

Fig. 9: Secondary electron images detailing the morphology of spinel grains from the Modderfontein Complex. (a) 120 µm diameter group 1 spinel from the northern domain (sample JB16-16; Fig. 2),

with altered rim (of group 2 spinel composition) < 20 µm thick. (b) 110 µm diameter group 2 spinel from the southern domain (JB16-33; see Fig. 2). White scale bar = 50 µm.

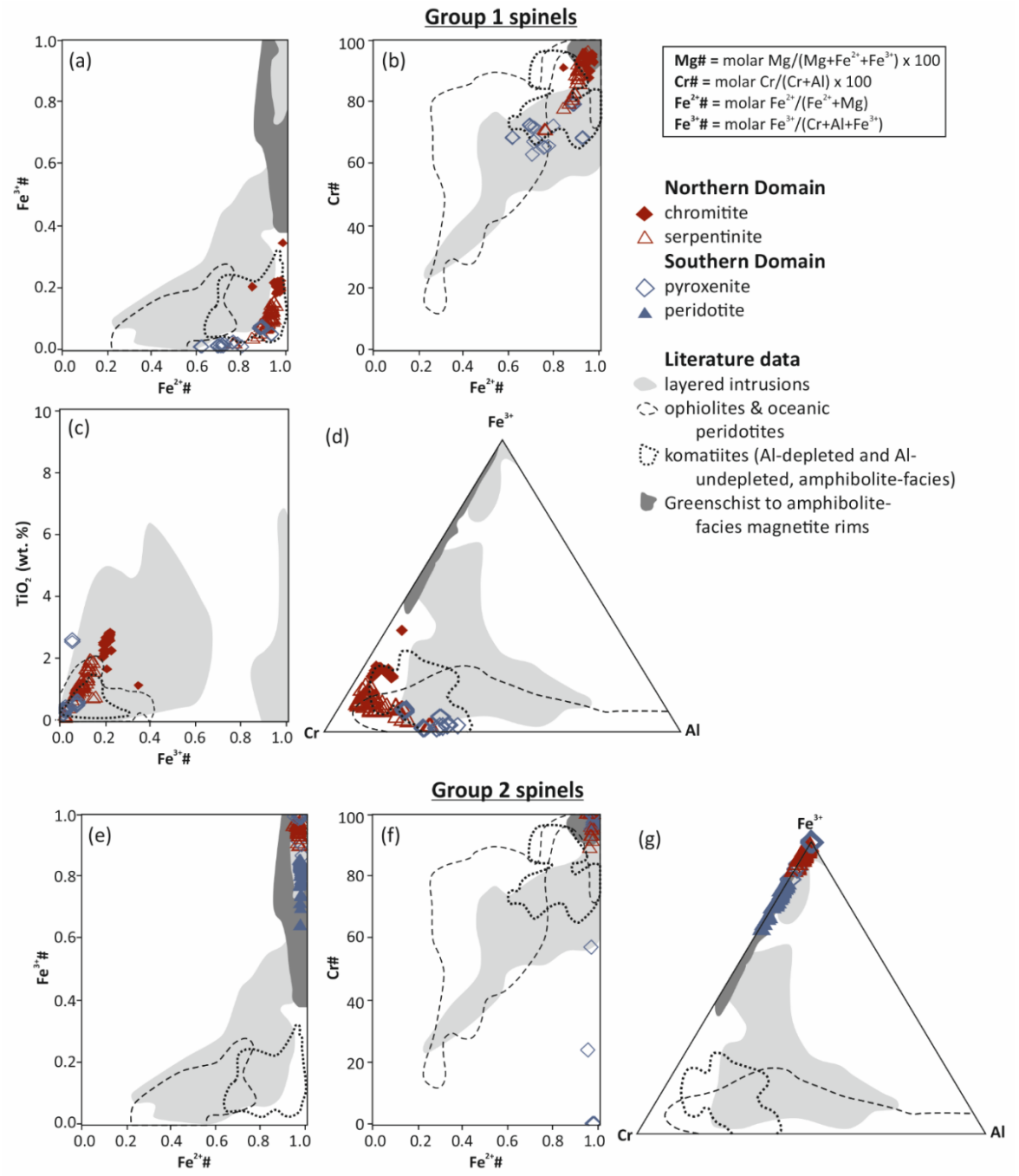

Fig. 10: Group 1 and 2 spinel compositions for the northern and southern domains of the Modderfontein Complex. Fields after: Barnes and Roeder (2001). Representative analyses can be found in Table 5 and the full dataset is available in the supplementary material.

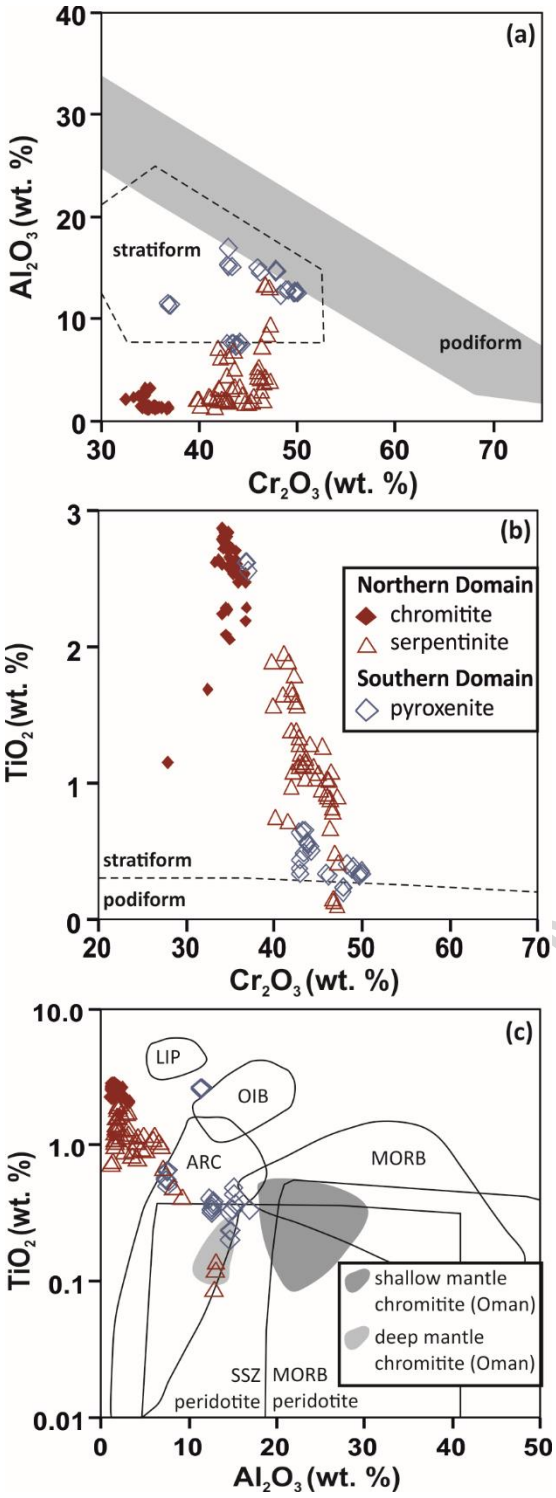

Fig. 11: Composition of the Group 1 spinel population (as outlined in text) on various discrimination diagrams. (a) Cr_2O_3 versus Al_2O_3 plot, with fields after Arai et al. (2004). (b) Al_2O_3 versus TiO_2 plots, with fields after Kamenetsky et al. (2001) and Rollinson (2008). (c) Cr_2O_3 versus TiO_2 plot, with fields Arai et al. (2004). Abbreviations: LIP = large igneous province; OIB = ocean island basalt; MORB = mid-ocean ridge basalt; SSZ = suprasubduction zone.

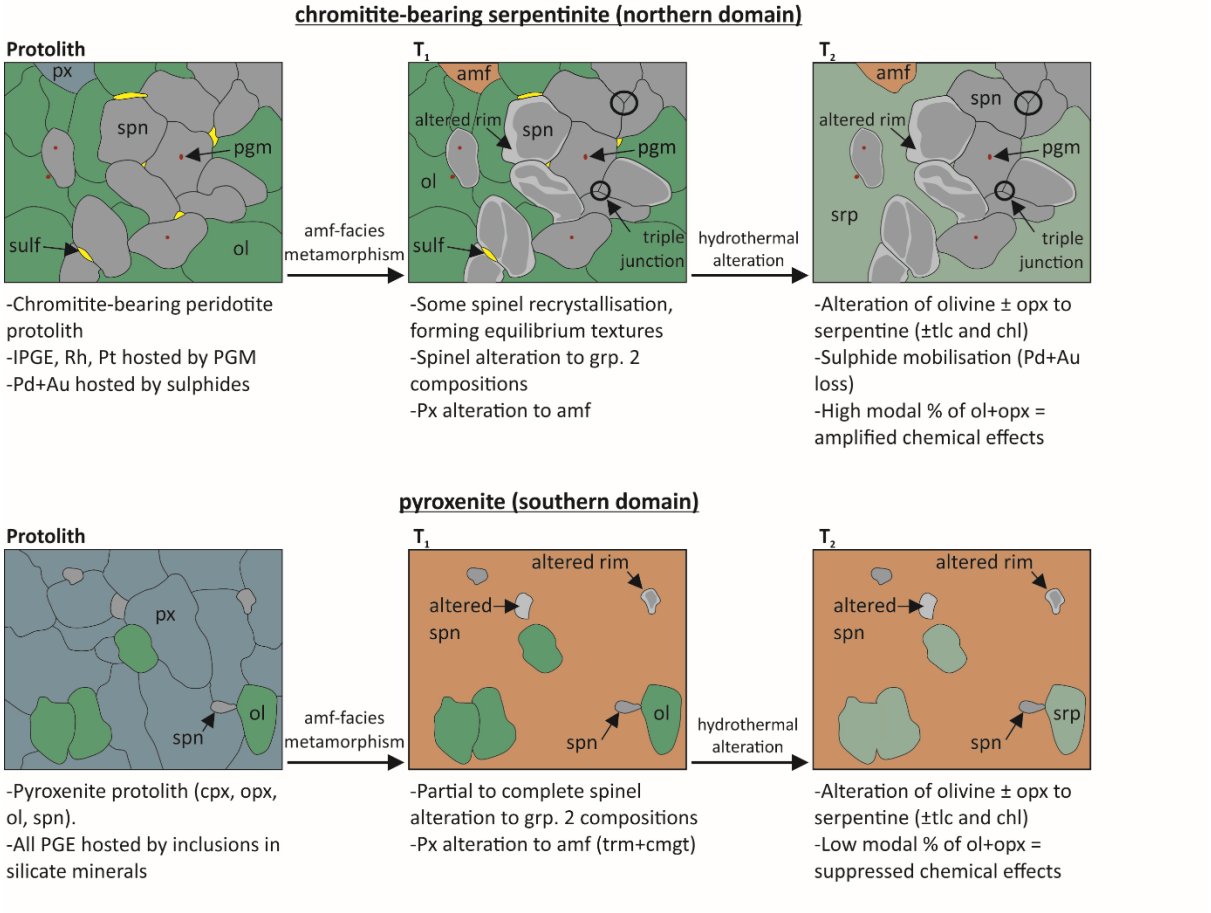

Fig. 12: Schematic diagrams summarising the microscopic petrographic and geochemical effects of amphibolite-facies metamorphism and hydrothermal alteration on the primary Modderfontein Rocks. Amf = amphibole; chl = chlorite; cmgt = cummingtonite; cpx = clinopyroxene; ol = olivine; PGM = platinum group mineral; px = pyroxenite; spn = spinel; srp = serpentine; sulph = base-metal sulphide; trm = tremolite.

TABLE CAPTIONS

Table 1: Summary of some proposed Archaean ophiolites from the North Atlantic, North China and Dharwar Cratons. Abbreviations: SSZ = suprasubduction zone

Name	Age (Ga)	Size (km^2)	Lithological assemblage	Metamorphic grade	Interpret-ation	Key evidence cited	Key references
North Atlantic Craton - Greenland							
Ivissartoq-Ujarassuit	3.08	~22	Pillow lava, volcanic breccia, picritic clinopyroxene cumulate, gabbro-diorite dyke, serpentinite, actinolite schist, anorthosite/leucogabbro, calc-silicate rocks, felsic schists	Amphibolite-facies	SSZ ophiolite	- Lithological assemblage similar to Phanerozoic (forearc) ophiolites - Trace element characteristics of the least altered samples, including negative HFSE anomalies and LILE enrichment	(Polat et al. 2008, Ordóñez-calderón et al. 2009)
Tartoq	3.19	~50	Pillow lava, gabbro, serpentinite, talc-schist, greenschist, amphibolite	Greenschist- to granulite-facies	SSZ ophiolite	- Trace element characteristics , including similarity to Phanerozoic arc-related rocks and negative HFSE anomalies. - Lithological assemblage comparable to oceanic crust - Structural studies suggesting that Tartoq was accreted in a convergent margin	(Kisters and Szilas 2012, Szilas et al. 2013, 2014)
Isua	3.80 - 3.70	87	Metabasalt, metagabbro, ultramafic rocks.	Amphibolite-facies	SSZ ophiolite	- It "contains all the major lithological units of a typical Penrose type complete ophiolite sequence" (Furnes et al. 2009). - O isotopes and petrographic features consistent with sea-floor hydrothermal alteration.	(Furnes et al. 2007a, 2007b, Friend and Nutman 2010, Hoffmann et al. 2010)
North China Craton							
Dongwanzi-Zunhua	2.51	~350	Banded Iron Formation, pillow lava, picritic amphibolites, gabbro, pyroxenite, cumulate ultramafic rocks (serpentinised dunite, pryoxenite, wehrlite and harzburgite), podiform chromitite	Amphibolite-facies	SSZ ophiolite	- Lithological assemblage comparable to Phanerozoic ophiolites. - Geochemistry of chromitites.	(Kusky et al. 2001, 2007, Zhao et al. 2007, 2008, Kusky and Jianghai 2010)
Dharwar Craton							
Devanur	2.53	80	Websterite, gabbro, mafic dykes, amphibolite, trondhjemite and pegmatite	Granulite-facies	SSZ ophiolite	- Trace element geochemistry, including negative HFSE anomalies and associated LILE enrichment.	(Yellappa et al. 2012)

Table 2: Bulk-rock major and trace element data for the Modderfontein Complex samples.

Abbreviations: am = amphibolite; cr = chromitite-bearing serpentinite; gb = gabbro; per = peridotite; px = pyroxenite; srp = serpentinite.

Sample	JB16-13	JB16-14	JB16-15	JB16-16	JB16-17	JB16-18	JB16-19	JB16-19CR	JB16-20	JB16-21	JB16-22
Domain	N	N	N	N	N	N	N	N	N	N	N
Lithology	srp	srp	srp	srp	srp	srp	srp	cr	srp	srp	srp
Major elements (wt. %)											
SiO_2	39.97	38.57	38.08	39.40	39.98	37.53	40.49	30.77	40.75	39.27	38.36
TiO_2	0.04	0.06	0.08	0.08	0.10	0.06	0.07	0.37	0.08	0.05	0.05
Al_2O_3	1.32	1.44	1.37	2.02	3.05	1.41	1.15	3.89	0.92	0.80	1.05
Fe_2O_3	9.64	10.07	11.00	8.09	8.14	7.48	13.12	19.51	13.87	10.75	9.86
MnO	0.14	0.17	0.14	0.11	0.09	0.08	0.20	0.53	0.18	0.14	0.10
MgO	37.75	37.50	37.72	37.43	35.38	35.51	34.56	28.55	37.25	38.14	38.10
CaO	0.01	0.09	0.05	0.57	0.95	0.07	0.05	0.12	0.13	0.06	0.13
Na_2O	0.02	0.03	0.02	0.01	0.03	0.02	0.03	0.07	0.08	0.03	0.04
K2O	0.02	0.03	0.02	0.03	0.02	0.03	0.02	0.03	0.03	0.01	0.02
P_2O_5	0.01	0.10	0.03	0.06	0.02	0.00	0.01	0.01	0.02	0.03	0.01
Cr_2O_3	0.44	0.63	0.32	0.66	0.67	0.68	0.39	8.32	0.73	0.48	0.45
LOI	11.18	11.58	11.01	12.11	11.80	16.88	11.13	8.39	7.12	10.28	12.21
Trace elements (ppm)											
Sc	4.1	3.2	6.6	6.8	8.2	4.4	3.2	6.3	4.4	3.1	3.6
V	20.1	21.0	23.7	39.4	50.4	29.4	22.3	268.4	37.6	18.9	19.1
Co	130	127	130	111	100	103	133	192	162	134	113
Ni	2922	2807	2706	2366	2031	2696	2632	2177	2726	2292	2867
Cu	3.21	8.50	12.88	4.15	5.16	14.91	27.58	14.29	20.22	12.95	6.6
Zn	53.52	78.00	55.30	58.08	74.43	60.64	80.05	854.31	92.12	83.06	73.9
Ga	2.37	2.74	1.92	2.99	3.04	2.19	2.50	9.15	2.74	1.67	1.4
Ge	0.86	1.07	0.78	0.79	0.74	0.62	1.19	1.35	1.19	0.84	0.6
Rb	0.54	1.74	4.53	1.31	0.74	1.10	1.47	2.09	0.95	0.48	0.2
Sr	2.23	7.00	2.01	20.21	16.52	4.39	5.49	4.96	4.47	2.64	4.9
Y	2.81	2.00	2.73	2.31	2.48	2.63	1.45	1.03	1.56	1.56	2.3
Zr	2.67	21.44	4.67	9.22	4.42	17.08	6.03	4.04	3.65	3.72	2.8
Nb	0.50	0.60	0.63	0.76	0.55	0.68	0.47	0.48	0.51	0.40	0.51
Cs	0.44	1.11	3.64	1.68	1.73	0.58	0.48	0.59	0.33	0.21	0.09
Ba	42.69	47.46	28.53	55.95	154.92	51.44	51.17	31.88	101.52	69.36	29.7
La	1.40	1.34	0.84	1.72	1.63	1.55	0.90	0.61	1.63	1.37	1.21
Ce	2.77	2.68	2.31	3.85	3.72	2.78	1.74	1.54	2.95	3.00	2.33
Pr	0.45	0.30	0.28	0.45	0.43	0.49	0.22	0.18	0.34	0.40	0.28
Nd	1.88	1.31	1.27	1.84	1.81	2.14	0.99	0.86	1.39	1.60	1.20
Sm	0.47	0.33	0.38	0.38	0.42	0.49	0.27	0.20	0.32	0.34	0.28
Eu	0.11	0.09	0.06	0.15	0.08	0.10	0.09	0.06	0.08	0.10	0.10
Gd	0.37	0.28	0.33	0.33	0.37	0.43	0.19	0.17	0.26	0.27	0.24
Tb	0.07	0.04	0.06	0.06	0.06	0.07	0.04	0.03	0.04	0.04	0.04
Dy	0.39	0.29	0.43	0.37	0.43	0.41	0.23	0.19	0.26	0.26	0.31
Ho	0.08	0.06	0.09	0.07	0.08	0.09	0.04	0.04	0.05	0.05	0.06
Er	0.23	0.16	0.27	0.22	0.25	0.26	0.14	0.12	0.15	0.12	0.18
Tm	0.03	0.03	0.04	0.04	0.03	0.04	0.02	0.02	0.02	0.02	0.02
Yb	0.19	0.17	0.26	0.21	0.22	0.22	0.16	0.11	0.12	0.11	0.15
Lu	0.04	0.04	0.05	0.04	0.04	0.04	0.03	0.02	0.02	0.02	0.03
Hf	0.06	0.39	0.14	0.26	0.11	0.41	0.14	0.10	0.08	0.09	0.09
Ta	0.03	0.05	0.06	0.08	0.05	0.06	0.05	0.04	0.04	0.03	0.04
Pb	5.09	4.77	2.50	6.59	7.53	2.92	1.93	4.30	6.26	2.45	0.29

Th	0.59	0.56	0.31	0.39	0.21	0.30	0.19	0.35	0.21	0.18	0.13
U	0.03	0.07	0.03	0.06	0.02	0.04	0.02	0.02	0.05	0.04	0.02

Sample	**JB16-23**	**JB16-27**	**JB16-29**	**JB16-30**	**JB16-31**	**JB16-32**	**JB16-33**	**JB16-35**	**JB16-38**	**JB16-40**
Domain	N	S	S	S	S	S	S	S	S	S
Lithology	cr	gb	per	px	per	px	per	px	srp	amf
Major elements (wt. %)										
SiO_2	31.03	51.22	39.49	47.99	41.88	46.76	36.86	46.56	38.31	44.54
TiO_2	0.22	0.10	0.05	0.11	0.07	0.07	0.19	0.08	0.07	0.20
Al_2O_3	2.87	11.39	4.61	2.23	2.69	1.17	3.59	1.69	2.89	5.43
Fe_2O_3	16.45	6.86	7.18	6.64	9.39	7.45	7.48	7.97	9.39	9.52
MnO	0.41	0.14	0.14	0.19	0.18	0.16	0.13	0.13	0.12	0.12
MgO	33.21	13.99	34.70	26.24	33.00	29.25	36.15	30.53	36.30	27.30
CaO	0.21	10.89	2.25	10.94	3.13	8.00	1.89	6.48	1.50	5.74
Na_2O	0.09	0.88	0.13	0.25	0.17	0.21	0.19	0.12	0.07	0.61
K2O	0.04	1.10	0.04	0.03	0.03	0.02	0.03	0.02	0.02	0.07
P_2O_5	0.01	0.01	0.01	0.01	0.02	0.02	0.02	0.01	0.00	0.02
Cr_2O_3	6.96	0.13	0.34	0.35	0.45	0.32	0.50	0.45	0.28	0.33
LOI	9.24	2.99	10.64	4.51	8.56	5.78	13.56	5.98	11.77	5.56
Trace elements (ppm)										
Sc	7.8	25.3	15.2	34.8	19.2	27.5	7.3	30.2	12.8	21.5
V	134.4	80.2	55.1	86.0	55.1	71.8	54.1	70.7	52.2	104.7
Co	233	49	82	69	97	84	105	87	91	86
Ni	2675	275	1472	748	1197	787	1107	1292	1800	1316
Cu	25.9	48.99	6.95	8.71	13.35	25.81	36.35	11.33	6.05	14.48
Zn	409.5	44.98	64.83	43.82	76.50	35.40	57.91	70.58	61.09	117.34
Ga	6.1	6.90	3.02	2.75	2.35	1.79	4.95	2.04	2.36	5.06
Ge	0.9	0.88	0.65	1.01	0.88	0.95	0.78	0.90	0.78	1.04
Rb	1.2	82.16	0.69	2.50	1.52	0.70	1.35	1.76	0.52	1.46
Sr	3.8	188.13	10.83	16.32	10.89	10.00	14.90	9.26	10.26	26.75
Y	1.4	3.94	3.21	4.99	3.33	2.49	5.75	2.51	2.30	5.09
Zr	2.7	3.84	1.89	4.15	2.16	2.43	17.09	3.49	5.89	9.85
Nb	0.31	0.34	0.22	0.28	0.21	0.29	1.29	0.24	0.36	0.52
Cs	0.20	5.15	1.76	1.51	1.22	1.27	1.05	0.54	1.28	0.29
Ba	22.6	143.76	32.51	61.40	94.15	28.66	34.21	37.21	84.65	46.31
La	0.45	1.10	0.52	1.31	1.44	0.67	1.68	0.97	0.58	1.00
Ce	1.15	2.10	1.25	2.78	2.05	1.68	4.25	2.48	1.19	2.01
Pr	0.13	0.31	0.11	0.44	0.34	0.18	0.56	0.31	0.11	0.35
Nd	0.58	1.48	0.44	1.82	1.36	0.97	2.60	1.32	0.53	1.61
Sm	0.19	0.46	0.13	0.63	0.36	0.31	0.76	0.37	0.19	0.52
Eu	0.07	0.22	0.05	0.21	0.08	0.12	0.25	0.12	0.07	0.19
Gd	0.17	0.45	0.19	0.69	0.47	0.32	0.79	0.39	0.20	0.65
Tb	0.03	0.08	0.05	0.12	0.08	0.06	0.14	0.07	0.04	0.12
Dy	0.20	0.62	0.37	0.82	0.52	0.38	0.90	0.47	0.32	0.85
Ho	0.04	0.13	0.09	0.16	0.11	0.08	0.17	0.09	0.06	0.18
Er	0.15	0.38	0.34	0.48	0.34	0.24	0.54	0.28	0.23	0.57
Tm	0.02	0.06	0.06	0.07	0.05	0.04	0.08	0.03	0.03	0.08
Yb	0.15	0.39	0.38	0.45	0.28	0.20	0.50	0.23	0.24	0.52
Lu	0.03	0.06	0.07	0.07	0.04	0.04	0.08	0.04	0.04	0.08
Hf	0.07	0.12	0.05	0.13	0.08	0.07	0.48	0.11	0.16	0.26
Ta	0.02	0.03	0.02	0.02	0.02	0.02	0.12	0.02	0.02	0.04
Pb	1.66	2.58	5.66	1.13	2.11	8.90	4.68	0.73	0.37	4.40
Th	0.13	0.10	0.05	0.07	0.04	0.05	0.41	0.12	0.04	0.09

U	0.01	0.01	0.01	0.01	0.01	0.02	0.06	0.02	0.01	0.01

Table 3: Bulk-rock platinum-group element and Au data for the Modderfontein Complex samples. Abbreviations: cr = chromitite-bearing serpentinite; per = peridotite; px = pyroxenite; Srp = serpentinite.

Sample	**JB16-13**	**JB16-15**	**JB16-19 CR**	**JB16-21**	**JB16-30**	**JB16-32**	**JB16-33**
Domain	N	N	N	N	S	S	S
Lithology	srp	srp	cr	srp	px	px	per
Platinum group-elements and Au (ppb)							
Os	0.81	0.73	23.53	0.32	0.36	0.09	0.16
Ir	0.86	0.57	23.69	0.29	0.48	0.17	0.25
Ru	5.83	6.68	59.42	4.07	3.36	1.44	1.54
Rh	0.97	0.64	83.98	0.39	1.92	0.87	0.91
Pt	3.96	4.45	93.28	1.73	13.95	14.35	7.74
Pd	4.51	1.21	2.87	1.85	4.93	16.34	10.08
Au	1.78	1.48	0.98	1.60	0.63	0.47	0.70

Table 4: Representative analyses of group 1 and 2 spinel from the Modderfontein Complex. The full dataset is available in the supplementary material.

	group 1 spinel									
Sample	**JB16-19**	**JB16-19**	**JB16-19**	**JB16-19**	**JB16-30**	**JB16-32**	**JB16-32**	**JB16-16**	**JB16-16**	**JB16-16**
Domain	N	N	N	N	S	S	S	N	N	N
Lithology	cr	cr	cr	cr	px	px	px	srp	srp	srp
SiO_2	0.15	0.15	0.15	0.17	0.21	0.24	0.19	0.21	0.21	0.24
TiO_2	2.54	2.29	2.74	2.27	0.20	0.33	0.53	0.08	1.17	1.32
Al_2O_3	1.17	2.49	1.40	1.08	14.66	12.64	7.63	12.91	3.14	1.78
FeO	51.34	52.14	52.57	53.60	25.73	28.21	41.62	30.68	42.29	43.74
Fe_2O_3	0.34	0.39	0.37	0.31	0.17	0.14	0.22	0.15	0.32	0.29
MnO	2.17	1.74	1.73	2.10	0.26	0.37	0.66	0.32	2.44	2.57
MgO	0.68	0.98	1.13	0.61	8.47	6.77	2.72	5.16	1.72	1.56
V_2O_3	0.59	0.39	0.57	0.57	0.24	0.34	0.46	0.20	0.44	0.42
Cr_2O_3	36.69	34.42	34.80	34.70	47.81	49.71	44.12	47.15	43.58	42.81
Total	95.66	95.00	95.45	95.40	97.75	98.75	98.15	96.86	95.31	94.72
Cations on the basis of 4 oxygens										
Si	0.01	0.01	0.01	0.01	0.01	0.01	0.01	0.01	0.01	0.01
Ti	0.08	0.07	0.09	0.07	0.01	0.01	0.01	0.00	0.04	0.04
Al	0.06	0.12	0.07	0.05	0.59	0.51	0.34	0.54	0.15	0.09
Fe^{2+}	1.33	1.33	1.34	1.35	0.69	0.77	1.11	0.85	1.16	1.20
Fe^{3+}	0.30	0.32	0.32	0.35	0.02	0.03	0.13	0.04	0.17	0.20
Mn	0.08	0.06	0.06	0.07	0.01	0.01	0.02	0.01	0.08	0.09
Mg	0.04	0.06	0.07	0.04	0.43	0.35	0.15	0.27	0.10	0.09
V	0.02	0.01	0.02	0.02	0.01	0.01	0.01	0.01	0.01	0.01
Cr	1.20	1.13	1.14	1.15	1.28	1.35	1.30	1.32	1.38	1.38
Total	3.11	3.12	3.12	3.12	3.04	3.03	3.08	3.04	3.09	3.10

Mg#	2.51	3.54	4.03	2.20	37.39	30.30	10.90	23.41	7.17	6.37
Cr#	95.46	90.25	94.35	95.58	68.63	72.51	79.50	71.02	90.31	94.18
Fe^{2+}#	0.97	0.96	0.95	0.97	0.62	0.69	0.88	0.76	0.92	0.93
Fe^{3+}#	0.19	0.20	0.21	0.23	0.01	0.01	0.07	0.02	0.10	0.12

	group 2 spinel									
Sample	**JB16-33**	**JB16-33**	**JB16-33**	**JB16-33**	**JB16-33**	**JB16-32**	**JB16-32**	**JB16-32**	**JB16-16**	**JB16-16**
Domain	S	S	S	S	S	S	S	S	N	N
Lithology	per	per	per	per	per	px	px	px	srp	srp
SiO_2	0.26	0.21	0.32	0.28	0.30	0.34	0.21	0.62	0.24	0.28
TiO_2	0.35	0.25	0.15	0.18	0.15	0.10	0.05	0.07	0.00	0.00
Al_2O_3	0.23	0.23	0.09	0.08	0.00	0.00	0.13	0.19	0.00	0.00
FeO	80.86	82.13	82.54	82.67	84.02	88.65	84.82	85.98	84.30	88.32
Fe_2O_3	0.32	0.32	0.34	0.29	0.36	0.00	0.34	0.38	0.00	0.00
MnO	0.39	0.28	0.26	0.30	0.18	0.12	0.21	0.14	0.13	0.09
MgO	0.33	0.27	0.38	0.36	0.35	0.28	0.20	0.27	0.41	0.41
V_2O_3	0.36	0.33	0.21	0.29	0.26	0.00	0.08	0.00	0.00	0.00
Cr_2O_3	9.59	8.27	7.50	7.53	6.83	0.32	5.85	4.09	4.74	1.34
Total	92.67	92.29	91.80	91.98	92.44	89.81	91.89	91.73	89.82	90.45
Cations on the basis of 4 oxygens										
Si	0.01	0.01	0.02	0.01	0.01	0.02	0.01	0.03	0.01	0.01
Ti	0.01	0.01	0.01	0.01	0.01	0.00	0.00	0.00	0.00	0.00
Al	0.01	0.01	0.01	0.00	0.00	0.00	0.01	0.01	0.00	0.00
Fe^{2+}	1.27	1.24	1.22	1.22	1.20	1.04	1.17	1.16	1.14	1.06
Fe^{3+}	1.36	1.44	1.48	1.48	1.53	1.91	1.60	1.64	1.67	1.86
Mn	0.02	0.01	0.01	0.01	0.01	0.01	0.01	0.01	0.01	0.00
Mg	0.02	0.02	0.03	0.03	0.03	0.02	0.01	0.02	0.03	0.03
V	0.01	0.01	0.01	0.01	0.01	0.00	0.00	0.00	0.00	0.00
Cr	0.37	0.32	0.30	0.30	0.27	0.01	0.23	0.16	0.19	0.06
Total	3.10	3.09	3.08	3.08	3.08	3.02	3.07	3.06	3.06	3.03
Mg#	0.91	0.73	1.04	0.99	0.94	0.74	0.54	0.71	1.12	1.09
Cr#	96.59	96.07	98.16	98.53	100.00	100.00	96.74	93.56	100.00	100.00
Fe^{2+}#	0.98	0.98	0.98	0.98	0.98	0.98	0.99	0.98	0.97	0.97
Fe^{3+}#	0.78	0.81	0.83	0.83	0.85	0.99	0.87	0.90	0.90	0.97

Table 5: Summary of the platinum-group mineral species and mineralogical associations found in the Modderfontein chromitite (sample JB16-19Cr).

Mineral	**Chemical Formula**	**Number identified**	**Mineralogical association**				**Grain size (µm)**		
			Silicate-Chromite boundary	*Chromite*	*Silicate blades in chromite*	*Silicate*	*Max*	*Min*	*Average*
Erlichmanite	OsS_2	7	2	5	0	0	4	0.8	2.1
Laurite	RuS_2	6	1	4	1	0	2	0.2	1.0
Sperrylite	$PtAs_2$	3	0	1	1	1	1.0	0.4	0.6
Platarsite	PtAsS	1	0	1	0	0	2.0	2.0	2.0
Platarsite-Hollingworthite	PtAsS-RhAsS	1	0	1	0	0	0.9	0.9	0.9

Hollingworthite-Irarsite	RhAsS IrAsS	1	0	0	1	0	1.0	1.0	1.0
Irarsite	IrAsS	1	0	1	0	0	0.5	0.5	0.5
TOTAL		*20*	*3*	*13*	*3*	*1*			

Highlights

- The Complex comprises lithologically distinctive domains separated by a shear zone
- Chromitite lenses are geochemically distinct from Phanerozoic podiform chromitite
- It is unlikely that the Modderfontein Complex represents an ophiolite fragment
- The Complex likely represents the intrusive remnant of a greenstone belt

Graphical abstract

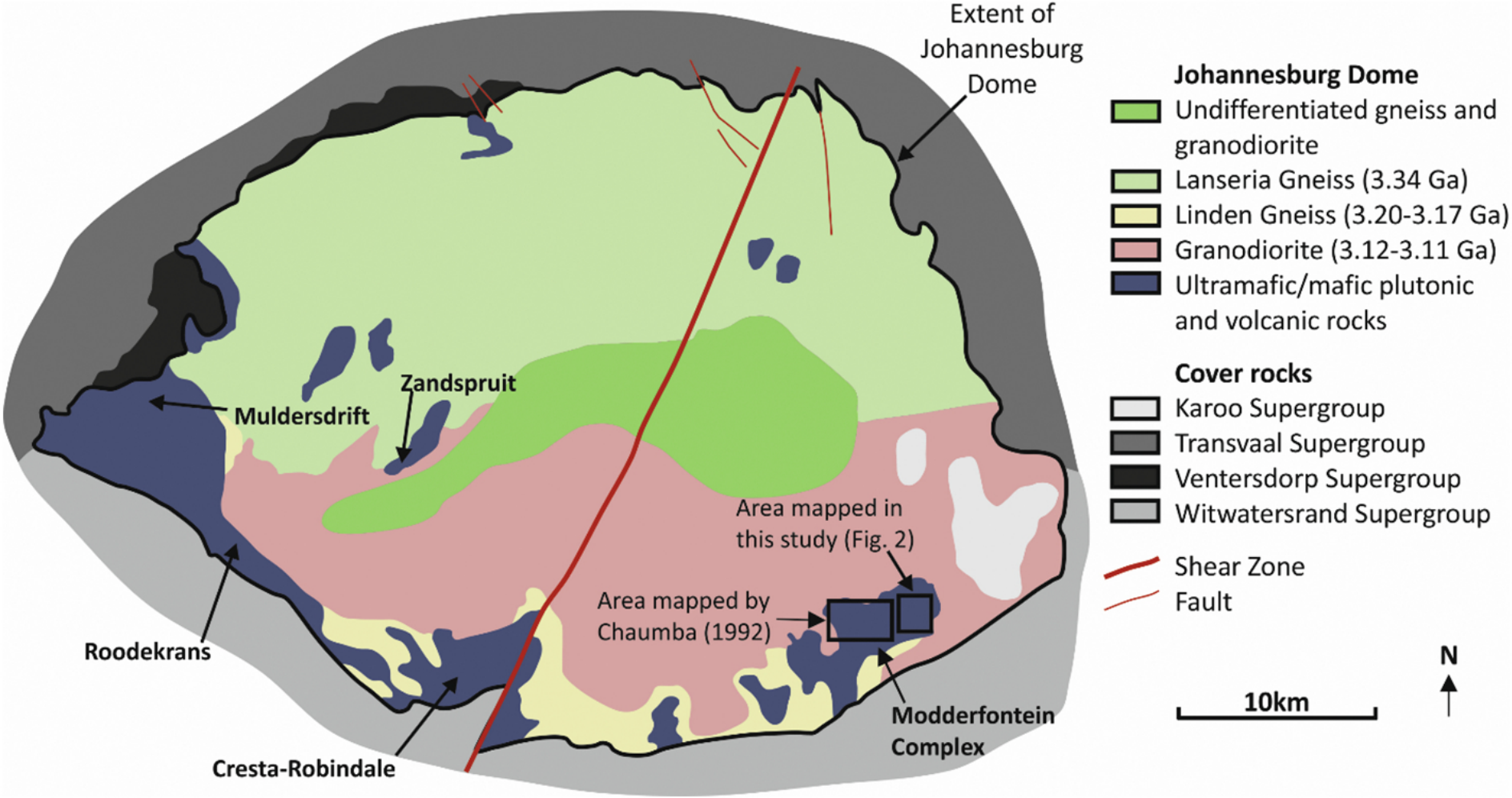
Extent of Johannesburg Dome
Johannesburg Dome
Undifferentiated gneiss and granodiorite
Lanseria Gneiss (3.34 Ga)
Linden Gneiss (3.20-3.17 Ga)
Granodiorite (3.12-3.11 Ga)
Ultramafic/mafic plutonic and volcanic rocks
Cover rocks
Karoo Supergroup
Transvaal Supergroup
Ventersdorp Supergroup
Witwatersrand Supergroup
Shear Zone
Fault
Muldersdrift
Zandspruit
Area mapped in this study (Fig. 2)
Area mapped by Chaumba (1992)
Roodekrans
Cresta-Robindale
Modderfontein Complex
10km
N

Figure 1

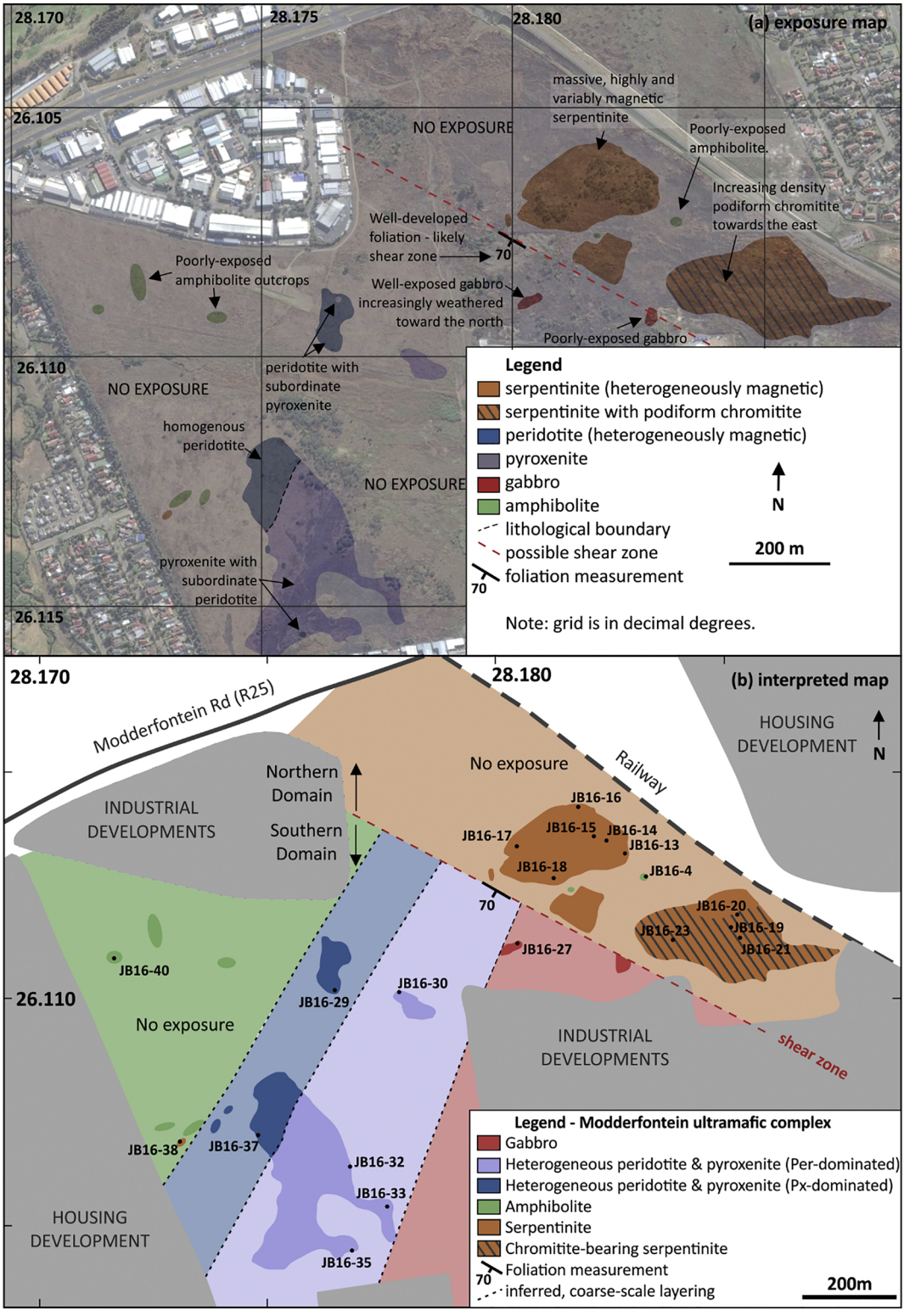
28.170
28.175
28.180
(a) exposure map
26.105
NO EXPOSURE
massive, highly and variably magnetic serpentinite
Poorly-exposed amphibolite.
Increasing density podiform chromitite towards the east
Well-developed foliation - likely shear zone
70
Poorly-exposed amphibolite outcrops
Well-exposed gabbro increasingly weathered toward the north
Poorly-exposed gabbro
26.110
NO EXPOSURE
peridotite with subordinate pyroxenite
homogenous peridotite
NO EXPOSURE
pyroxenite with subordinate peridotite
26.115
Legend
serpentinite (heterogeneously magnetic)
serpentinite with podiform chromitite
peridotite (heterogeneously magnetic)
pyroxenite
gabbro
amphibolite
lithological boundary
possible shear zone
foliation measurement
70
N
200 m
Note: grid is in decimal degrees.
28.170
28.180
(b) interpreted map
Modderfontein Rd (R25)
HOUSING DEVELOPMENT
N
Railway
No exposure
Northern Domain
Southern Domain
INDUSTRIAL DEVELOPMENTS
JB16-16
JB16-17
JB16-15
JB16-14
JB16-13
JB16-18
JB16-4
70
JB16-20
JB16-23
JB16-19
JB16-21
JB16-27
JB16-40
JB16-30
JB16-29
26.110
No exposure
INDUSTRIAL DEVELOPMENTS
shear zone
JB16-38
JB16-37
JB16-32
JB16-33
HOUSING DEVELOPMENT
JB16-35
Legend - Modderfontein ultramafic complex
Gabbro
Heterogeneous peridotite & pyroxenite (Per-dominated)
Heterogeneous peridotite & pyroxenite (Px-dominated)
Amphibolite
Serpentinite
Chromitite-bearing serpentinite
Foliation measurement
70
inferred, coarse-scale layering
200m

Figure 2

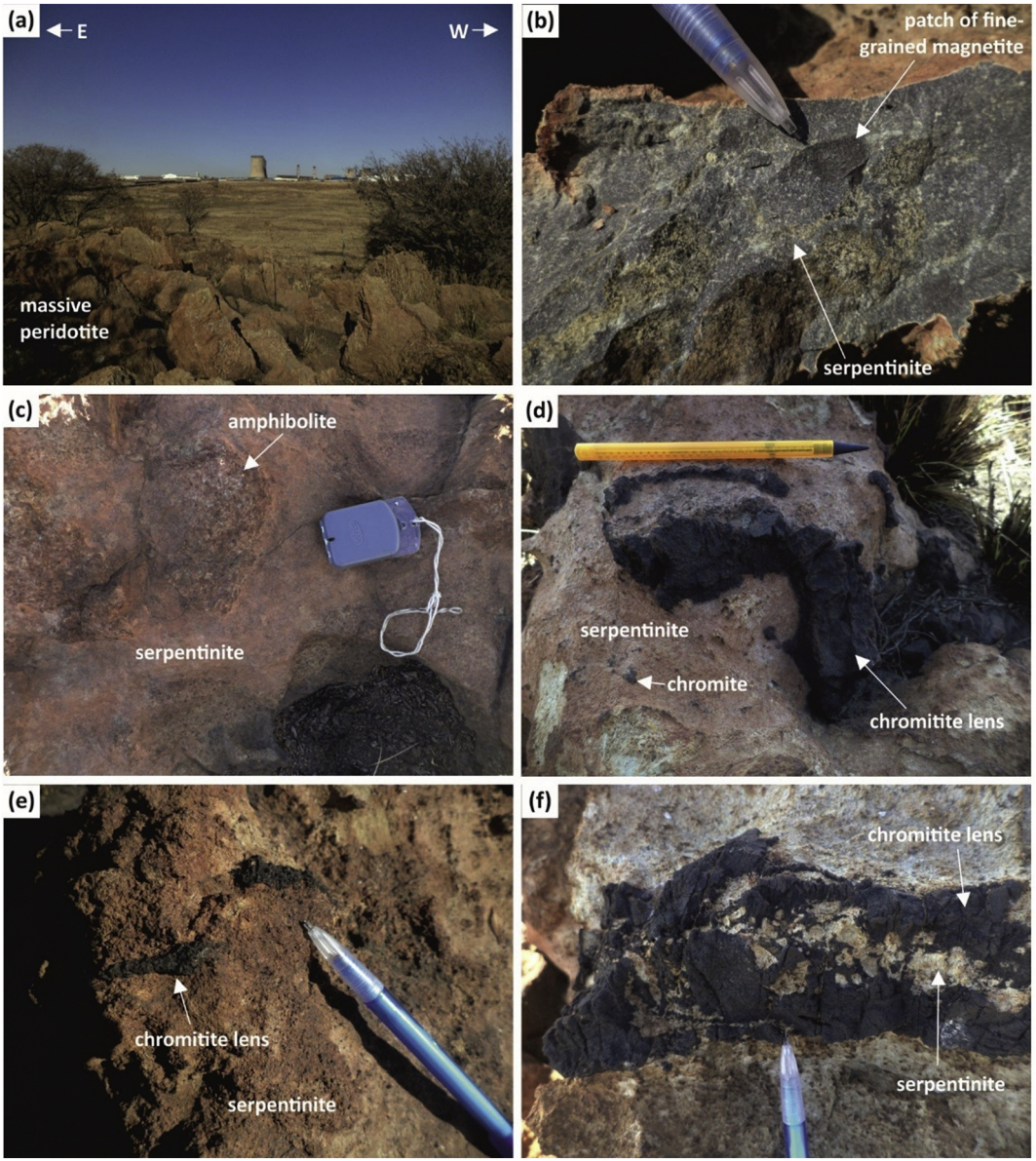
(a)
E
W
massive peridotite
(b)
patch of fine-grained magnetite
serpentinite
(c)
amphibolite
serpentinite
(d)
serpentinite
chromite
chromitite lens
(e)
chromitite lens
serpentinite
(f)
chromitite lens
serpentinite

Figure 3

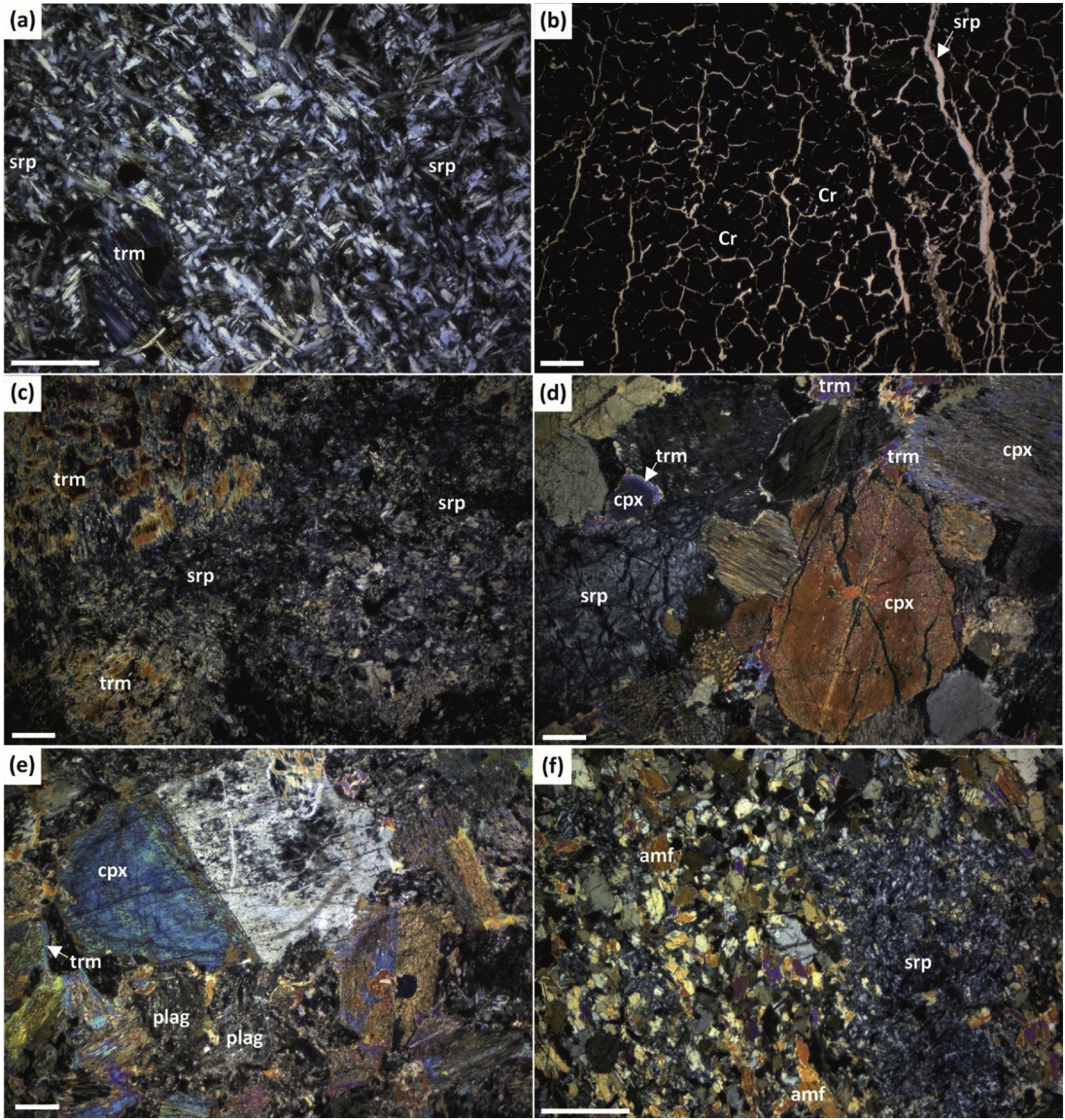
(a)
srp
srp
trm
(b)
srp
Cr
Cr
(c)
trm
srp
srp
trm
(d)
trm
trm
trm
cpx
cpx
srp
cpx
(e)
cpx
trm
plag
plag
(f)
amf
srp
amf

Figure 4

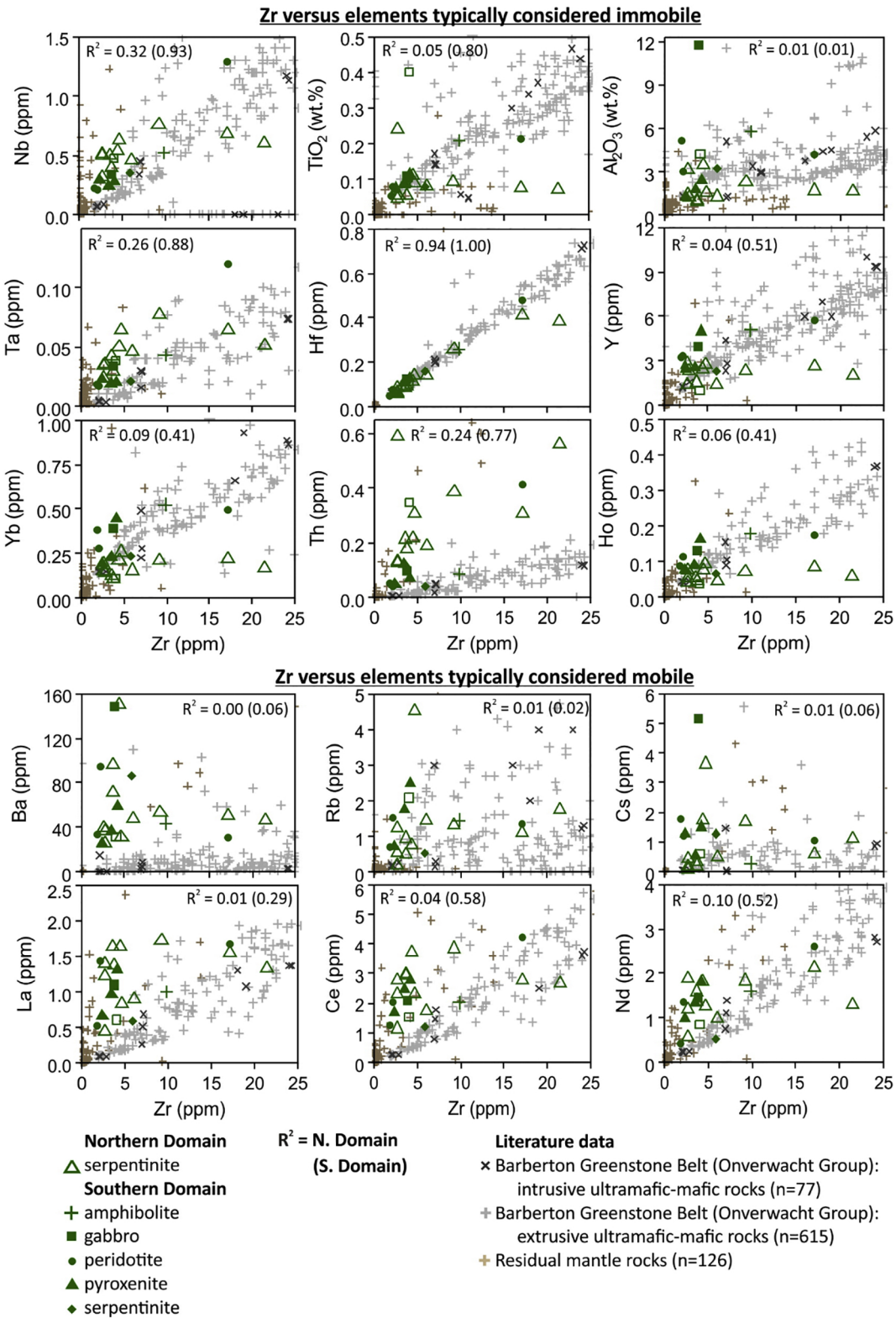
Zr versus elements typically considered immobile
Nb (ppm)
R² = 0.32 (0.93)
TiO2 (wt.%)
R² = 0.05 (0.80)
Al2O3 (wt.%)
R² = 0.01 (0.01)
Ta (ppm)
R² = 0.26 (0.88)
Hf (ppm)
R² = 0.94 (1.00)
Y (ppm)
R² = 0.04 (0.51)
Yb (ppm)
R² = 0.09 (0.41)
Th (ppm)
R² = 0.24 (0.77)
Ho (ppm)
R² = 0.06 (0.41)
Zr (ppm)
Zr versus elements typically considered mobile
Ba (ppm)
R² = 0.00 (0.06)
Rb (ppm)
R² = 0.01 (0.02)
Cs (ppm)
R² = 0.01 (0.06)
La (ppm)
R² = 0.01 (0.29)
Ce (ppm)
R² = 0.04 (0.58)
Nd (ppm)
R² = 0.10 (0.52)
Zr (ppm)
Northern Domain
serpentinite
Southern Domain
amphibolite
gabbro
peridotite
pyroxenite
serpentinite
R² = N. Domain
(S. Domain)
Literature data
Barberton Greenstone Belt (Onverwacht Group): intrusive ultramafic-mafic rocks (n=77)
Barberton Greenstone Belt (Onverwacht Group): extrusive ultramafic-mafic rocks (n=615)
Residual mantle rocks (n=126)

Figure 5

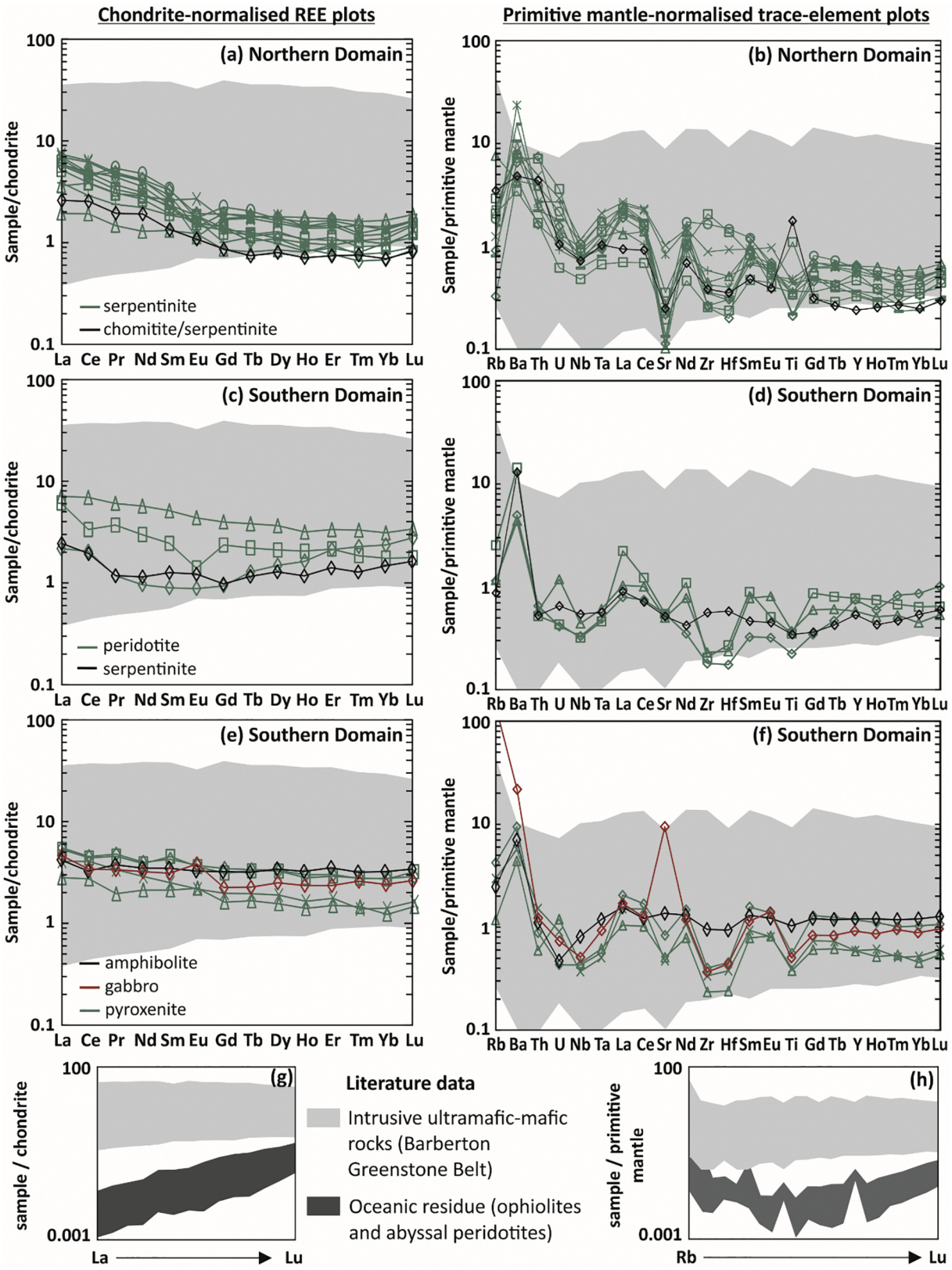
Chondrite-normalised REE plots
Primitive mantle-normalised trace-element plots
(a) Northern Domain
(b) Northern Domain
(c) Southern Domain
(d) Southern Domain
(e) Southern Domain
(f) Southern Domain
Sample/chondrite
Sample/primitive mantle
100
10
1
0.1
La Ce Pr Nd Sm Eu Gd Tb Dy Ho Er Tm Yb Lu
Rb Ba Th U Nb Ta La Ce Sr Nd Zr Hf Sm Eu Ti Gd Tb Y Ho Tm Yb Lu
serpentinite
chromitite/serpentinite
peridotite
serpentinite
amphibolite
gabbro
pyroxenite
(g)
(h)
sample / chondrite
sample / primitive mantle
0.001
La
Lu
Rb
Literature data
Intrusive ultramafic-mafic rocks (Barberton Greenstone Belt)
Oceanic residue (ophiolites and abyssal peridotites)

Figure 6

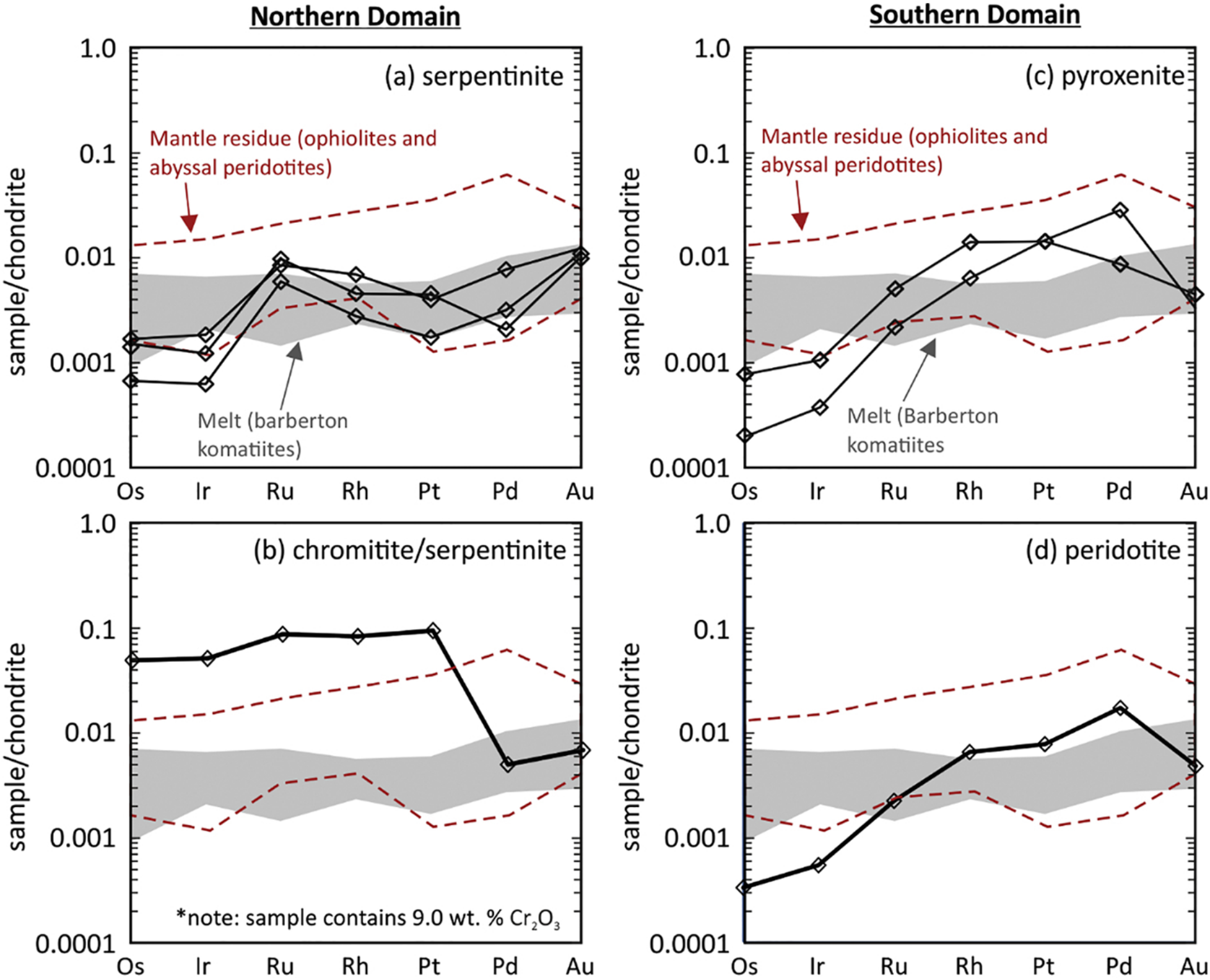
Northern Domain
Southern Domain
(a) serpentinite
(c) pyroxenite
(b) chromitite/serpentinite
(d) peridotite
Mantle residue (ophiolites and abyssal peridotites)
Melt (barberton komatiites)
Melt (Barberton komatiites
*note: sample contains 9.0 wt. % Cr_2O_3
sample/chondrite
1.0
0.1
0.01
0.001
0.0001
Os
Ir
Ru
Rh
Pt
Pd
Au

Figure 7

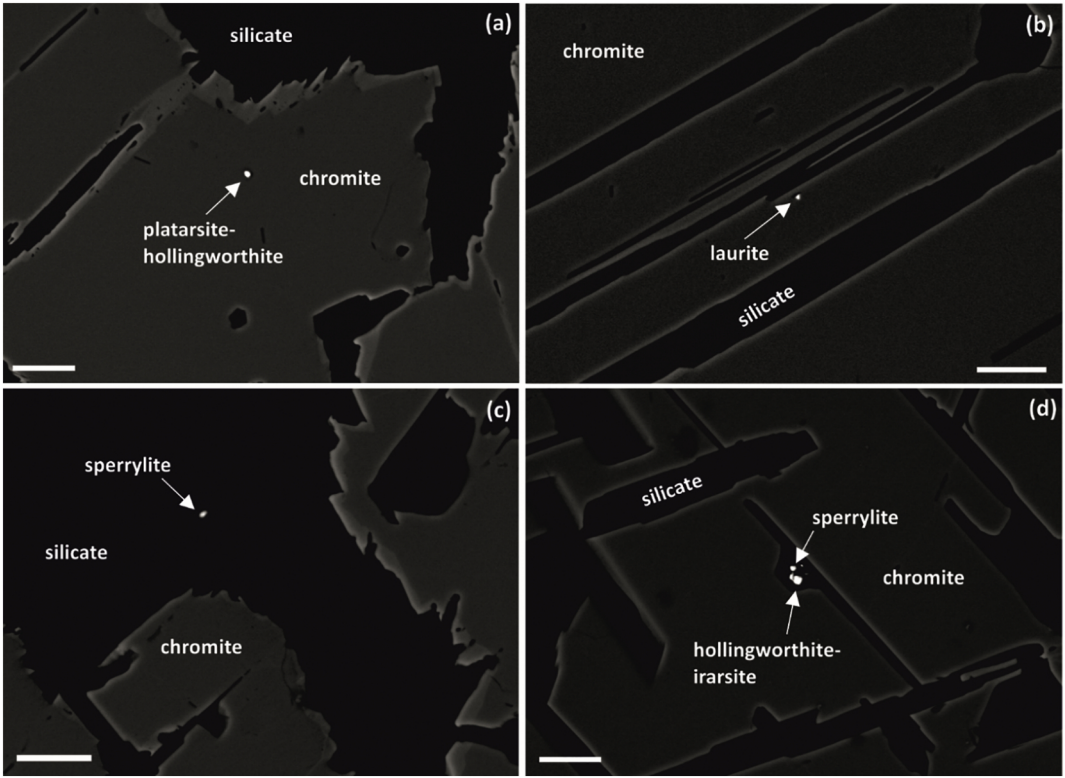
(a)
silicate
chromite
platarsite-
hollingworthite
(b)
chromite
laurite
silicate
(c)
sperrylite
silicate
chromite
(d)
silicate
sperrylite
chromite
hollingworthite-
irarsite

Figure 8

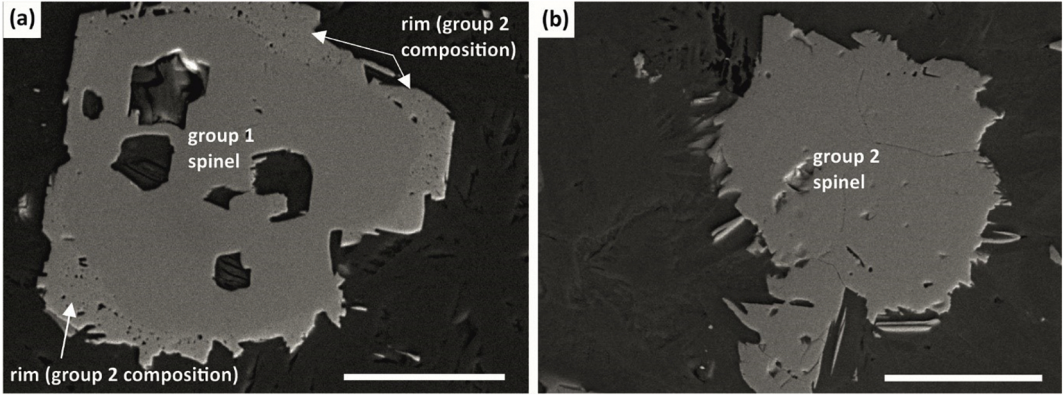
(a)
rim (group 2 composition)
group 1 spinel
rim (group 2 composition)
(b)
group 2 spinel

Figure 9

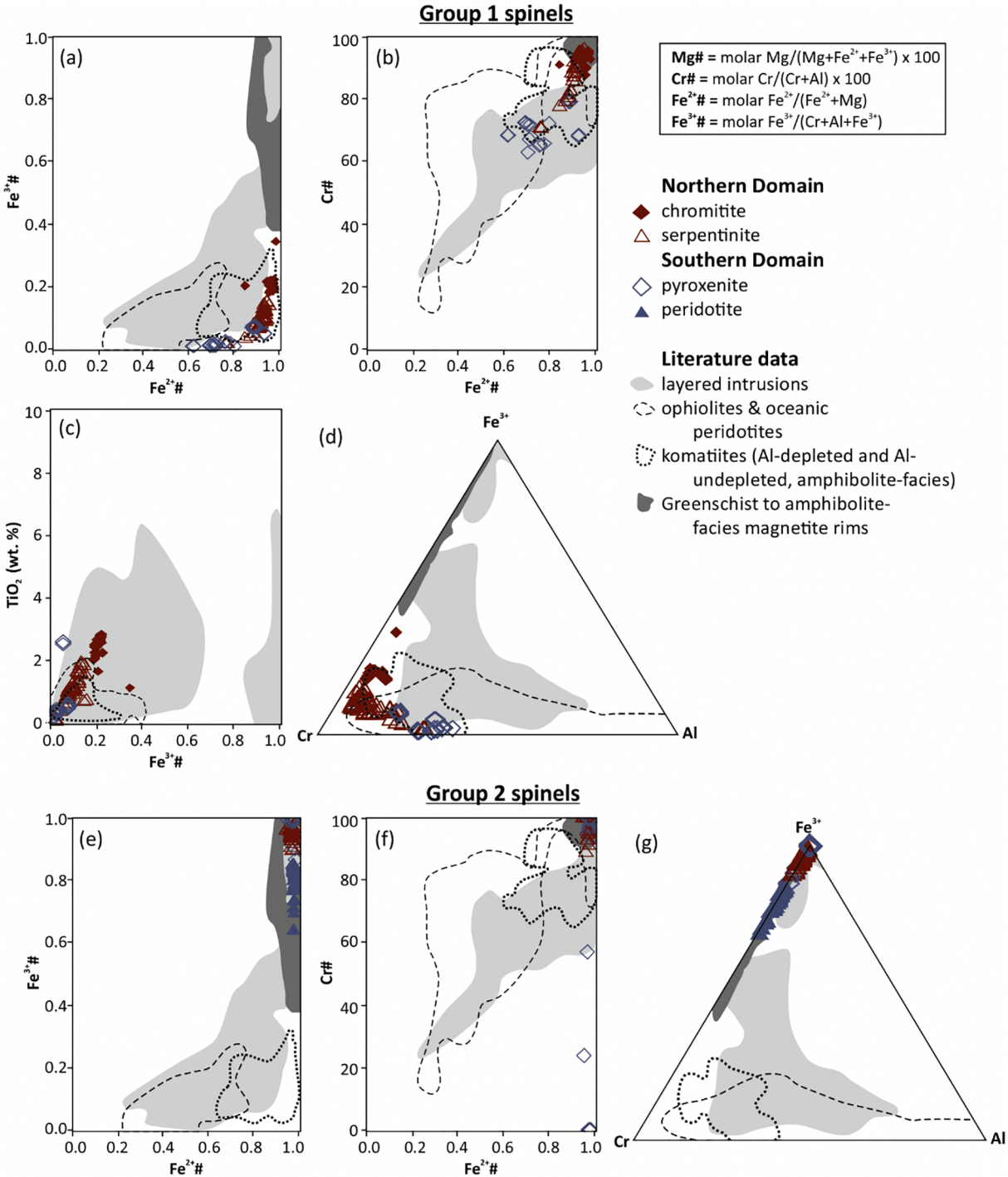
Group 1 spinels
(a)
(b)
(c)
(d)
Fe3+#
Fe2+#
Cr#
TiO2 (wt. %)
Fe3+
Cr
Al
Mg# = molar Mg/(Mg+Fe2+ +Fe3+) x 100
Cr# = molar Cr/(Cr+Al) x 100
Fe2+# = molar Fe2+/(Fe2+ +Mg)
Fe3+# = molar Fe3+/(Cr+Al+Fe3+)
Northern Domain
chromitite
serpentinite
Southern Domain
pyroxenite
peridotite
Literature data
layered intrusions
ophiolites & oceanic peridotites
komatiites (Al-depleted and Al-undepleted, amphibolite-facies)
Greenschist to amphibolite-facies magnetite rims
Group 2 spinels
(e)
(f)
(g)

Figure 10

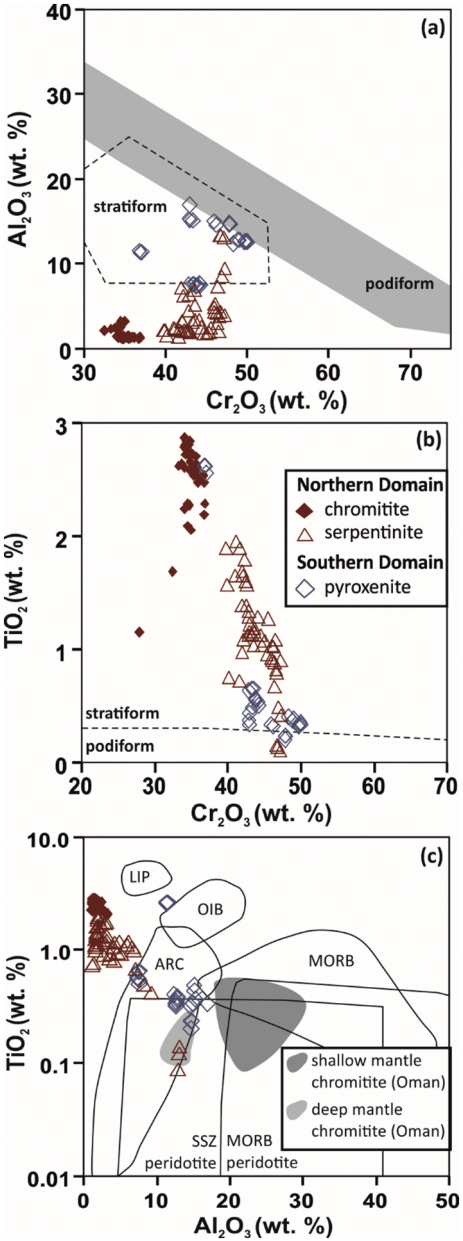
(a)
Al_2O_3 (wt. %)
Cr_2O_3 (wt. %)
stratiform
podiform
(b)
TiO_2 (wt. %)
Cr_2O_3 (wt. %)
Northern Domain
chromitite
serpentinite
Southern Domain
pyroxenite
stratiform
podiform
(c)
TiO_2 (wt. %)
Al_2O_3 (wt. %)
LIP
OIB
ARC
MORB
shallow mantle chromitite (Oman)
deep mantle chromitite (Oman)
SSZ peridotite
MORB peridotite

Figure 11

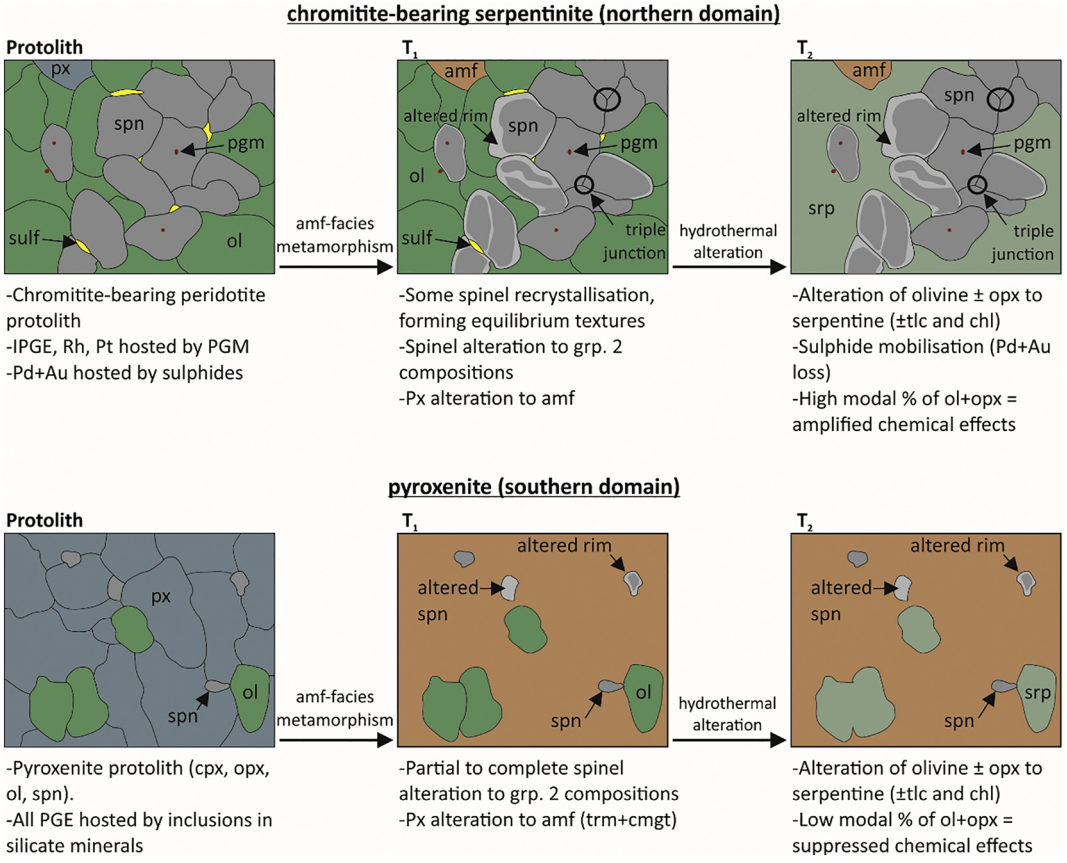
chromitite-bearing serpentinite (northern domain)
Protolith
px
spn
pgm
sulf
ol
amf-facies metamorphism
T1
amf
altered rim
spn
pgm
ol
sulf
triple junction
hydrothermal alteration
T2
amf
spn
altered rim
pgm
srp
triple junction
-Chromitite-bearing peridotite protolith
-IPGE, Rh, Pt hosted by PGM
-Pd+Au hosted by sulphides
-Some spinel recrystallisation, forming equilibrium textures
-Spinel alteration to grp. 2 compositions
-Px alteration to amf
-Alteration of olivine ± opx to serpentine (±tlc and chl)
-Sulphide mobilisation (Pd+Au loss)
-High modal % of ol+opx = amplified chemical effects
pyroxenite (southern domain)
Protolith
px
ol
spn
amf-facies metamorphism
T1
altered rim
altered spn
ol
spn
hydrothermal alteration
T2
altered rim
altered spn
srp
spn
-Pyroxenite protolith (cpx, opx, ol, spn).
-All PGE hosted by inclusions in silicate minerals
-Partial to complete spinel alteration to grp. 2 compositions
-Px alteration to amf (trm+cmgt)
-Alteration of olivine ± opx to serpentine (±tlc and chl)
-Low modal % of ol+opx = suppressed chemical effects

Figure 12